



HAL
open science

Controls on Alkenone Carbon Isotope Fractionation in the Modern Ocean

Samuel R Phelps, Heather M Stoll, Clara Bolton, Luc L Beaufort, Pratigya J Polissar

► **To cite this version:**

Samuel R Phelps, Heather M Stoll, Clara Bolton, Luc L Beaufort, Pratigya J Polissar. Controls on Alkenone Carbon Isotope Fractionation in the Modern Ocean. *Geochemistry, Geophysics, Geosystems*, 2021, 22 (12), pp.e2021GC009658. 10.1029/2021gc009658 . hal-03561622

HAL Id: hal-03561622

<https://hal.science/hal-03561622>

Submitted on 8 Feb 2022

HAL is a multi-disciplinary open access archive for the deposit and dissemination of scientific research documents, whether they are published or not. The documents may come from teaching and research institutions in France or abroad, or from public or private research centers.

L'archive ouverte pluridisciplinaire **HAL**, est destinée au dépôt et à la diffusion de documents scientifiques de niveau recherche, publiés ou non, émanant des établissements d'enseignement et de recherche français ou étrangers, des laboratoires publics ou privés.



RESEARCH ARTICLE

10.1029/2021GC009658

Controls on Alkenone Carbon Isotope Fractionation in the Modern Ocean

 Samuel R. Phelps^{1,2} , Heather M. Stoll³ , Clara T. Bolton⁴ , Luc Beaufort⁴ , and Pratyga J. Polissar^{5,6} 

¹Department of Earth and Environmental Sciences, Columbia University, New York, NY, USA, ²Department of Earth and Planetary Sciences, Harvard University, Cambridge, MA, USA, ³Department of Earth Sciences, ETH Zürich, Zürich, Switzerland, ⁴Aix-Marseille Université, CNRS, IRD, INRAE, Collège de France, CEREGE, Aix-en-Provence, France, ⁵Division of Biology and Paleo-Environment, Lamont-Doherty Earth Observatory of Columbia University, Palisades, NY, USA, ⁶Department of Ocean Sciences, University of Santa Cruz, Santa Cruz, CA, USA

Key Points:

- Irradiance is a primary control on alkenone carbon isotope fractionation in the natural environment
- Culture-calibrated model can predict alkenone carbon isotope fractionation in core-top sediment samples
- Diffusive model “*b*” value is not correlated with growth rate: diffusive model should not be used for paleobarometry

Supporting Information:

Supporting Information may be found in the online version of this article.

Correspondence to:

S. R. Phelps,
sphelps@fas.harvard.edu

Citation:

Phelps, S. R., Stoll, H. M., Bolton, C. T., Beaufort, L., & Polissar, P. J. (2021). Controls on Alkenone carbon isotope fractionation in the modern ocean. *Geochemistry, Geophysics, Geosystems*, 22, e2021GC009658. <https://doi.org/10.1029/2021GC009658>

Received 15 JAN 2021
Accepted 1 NOV 2021

Abstract Carbon isotope records from alkenone biomarkers ($\epsilon_{p37:2}$) produced by haptophyte algae are frequently used for atmospheric CO₂ paleobarometry, but this method has yielded inconsistent results during periods where CO₂ variations are known independently. Recent syntheses of algal cultures have quantitatively demonstrated that $\epsilon_{p37:2}$ indeed records CO₂ information: $\epsilon_{p37:2}$ increases as aqueous CO₂ concentrations increase relative to carbon demand. However, interpretations of $\epsilon_{p37:2}$ are complicated by irradiance, where higher irradiance yields higher $\epsilon_{p37:2}$. Here we examine the roles of physiology and environment in setting $\epsilon_{p37:2}$ in the ocean. We compile water-column and sediment core-top $\epsilon_{p37:2}$ data and add new core-top measurements, including estimates of cell sizes and growth rates of the alkenone-producing population. In support of culture studies, we find irradiance to be a key control on $\epsilon_{p37:2}$ in the modern ocean. We test a culture-derived model of $\epsilon_{p37:2}$ and find that the quantitative relationships calibrated in culture experiments can be used to predict $\epsilon_{p37:2}$ in sediment samples. In water-column samples, the model substantially overestimates $\epsilon_{p37:2}$, largely resulting from higher irradiance at the depth of sample collection than the integrated light conditions under which the sampled biomass was produced and vertically mixed to the collection depth. We argue that the theory underpinning the conventional diffusive alkenone carbon isotope fractionation model, including the “*b*” parameter, is not supported by field data and should not be used to reconstruct past CO₂ changes. Future estimates of CO₂ from $\epsilon_{p37:2}$ should use empirical or mechanistic models to quantitatively account for irradiance and cell size variations.

1. Introduction

Understanding the role of CO₂ as both a feedback on, and forcing of, global climate is essential for better predicting how present and future anthropogenic CO₂ emissions will shape life on Earth. Carbon isotope ($\delta^{13}\text{C}$) fractionation in photosynthetic organic matter has long been used to estimate ancient atmospheric CO₂ concentrations (e.g., Popp et al., 1989). The vast majority of carbon isotope-based CO₂ records are derived from long-chain alkenones, unsaturated ketones produced by the algal order Isochrysidales, whose modern coccolithophorid forms include the widespread genera *Gephyrocapsa* and *Emiliana*, as well as the less abundant *Reticulofenestra* (Bendif et al., 2016). Because of the constant isotopic offset between alkenone $\delta^{13}\text{C}$ and bulk cellular organic matter $\delta^{13}\text{C}$ (Popp, Kenig, et al., 1998; Riebesell, Revill, et al., 2000; Wilkes et al., 2018), these molecules are faithful recorders of the carbon isotope fractionation during photosynthesis (ϵ_p) in these algae. ϵ_p is calculated using Equation 1, where $\delta^{13}\text{C}_{\text{CO}_2\text{aq}}$ is the isotopic composition of aqueous CO₂, $\delta^{13}\text{C}_{\text{POC}}$ is the isotopic composition of algal organic matter (Freeman & Hayes, 1992), and reported on the VPDB scale in units of permil (‰).

$$\epsilon_p = 1000 \times \left(\left(\delta^{13}\text{C}_{\text{CO}_2\text{aq}} + 1000 \right) / \left(\delta^{13}\text{C}_{\text{POC}} + 1000 \right) - 1 \right) \quad (1)$$

Past field observations have shown that ϵ_p is related to the growth environment, including ambient CO₂ concentrations, temperature, and irradiance, as well as algal physiology (Francois et al., 1993; Fry & Wainwright, 1991; Laws et al., 1995; Popp, Laws, et al., 1998; Rau et al., 1992; Wolhowe et al., 2015). Variations in ϵ_p are classically interpreted in terms of changes in [CO_{2(aq)}] relative to cellular carbon demand and supply modulations, which include growth rate, cellular carbon content, and surface area, together approximated using the *b* parameter (Bidigare et al., 1997). These interpretations follow quantitative models of carbon isotope fractionation in land plants

© 2021. The Authors.

This is an open access article under the terms of the [Creative Commons Attribution-NonCommercial-NoDerivs License](https://creativecommons.org/licenses/by/4.0/), which permits use and distribution in any medium, provided the original work is properly cited, the use is non-commercial and no modifications or adaptations are made.

(Farquhar et al., 1982), which are governed by diffusive CO_2 supply and the relative expression of the kinetic isotope fractionation by the carboxylating enzyme Ribulose-1,5-bisphosphate carboxylase-oxygenase (RubisCO). Recent syntheses of culture data have elucidated the quantitative relationships between various physiological and environmental influences, and confirmed that ϵ_p does indeed decline as $[\text{CO}_{2(\text{aq})}]$ decreases (e.g., Phelps et al., 2021; Stoll et al., 2019). However, culture experiments suggest that light energy, independent of its effect on growth rate, is nearly as important a control on ϵ_p as physiology and CO_2 , with higher ϵ_p occurring at higher irradiance (Phelps et al., 2021; Rost et al., 2002; Stoll et al., 2019; Wilkes & Pearson, 2019). Though alkenone ϵ_p ($\epsilon_{p37:2}$, subscript representing the diunsaturated ketone with 37 carbon atoms) has been extensively used to generate paleo- CO_2 records, only two studies have quantitatively considered cell size, growth rate, and irradiance when interpreting alkenone ϵ_p in down-core sediment sequences (Stoll et al., 2019; Tanner et al., 2020). How these quantitative relationships observed in culture experiments can be transferred to the natural environment remains an area of active research (Hernández-Almeida et al., 2020).

Here we focus on the modern and late Holocene ocean and conduct an empirical analysis to test whether the same relationships between physiological and environmental parameters and alkenone ϵ_p identified in culture also hold true in the natural environment. We explore this question with a careful compilation of published alkenone $\delta^{13}\text{C}$ measurements from modern suspended particulate organic matter samples and from late Holocene core-tops, and add new alkenone $\delta^{13}\text{C}$ and coccolith size measurements from 22 core-top sediment samples. We estimate growth rates of the alkenone-producing algae using Michaelis-Menten parameterizations, and compile published coccolithophore assemblage and size data to estimate cellular carbon demand at each sample location. We examine the relationship between alkenone ϵ_p and carbon demand and carbon supply, as well as the direct influence of irradiance and nutrients on alkenone ϵ_p . We evaluate whether a multiple linear regression model of ϵ_p developed from cultures (Phelps et al., 2021) is applicable to the ocean, and test the theory of the conventional diffusive alkenone ϵ_p model using growth rate data.

2. Methods, Samples, and Data Sources

2.1. Alkenone ϵ_p Samples

Our sample set can be most broadly divided into “water-column” or “sediment” groups. Water-column samples, taken from suspended particulate organic matter in the water column (between 0 and 300 m depth), have all been previously reported (Figure 1a) (Benthien et al., 2007; Bidigare et al., 1997, 1999; Eek et al., 1999; Laws et al., 2001; Prahl et al., 2005; Wallsgrove, 2008; Wolfshorndl et al., 2019; Wolhowe et al., 2014, 2015). For inclusion in our compilation and analysis, particulate data must report (a) $\delta^{13}\text{C}$ values of the $\text{C}_{37:2}$ methyl ketone, (b) $[\text{CO}_{2(\text{aq})}]$ or $p\text{CO}_2$ during alkenone sampling, and (c) $\delta^{13}\text{C}_{\text{DIC}}$ during alkenone sampling. We exclude the suspended particulate data from five datasets (Gould et al., 2019; Harada et al., 2003; Schulte et al., 2003; Tolosa et al., 2008; Yamamoto et al., 2007) because they failed to meet one or more of these criteria, preventing accurate calculation of $\epsilon_{p37:2}$.

New core-top sediment samples ($n = 22$) come from the Lamont-Doherty Earth Observatory Core Repository (LDEO Repository). Several of these samples were obtained during the R/V Oceanus Cruise 437-7 along the NW African margin (McGee et al., 2013); the remainder come from various sediment cores in the LDEO Repository. We combine our new sediment data with published core-top data for analysis (Andersen et al., 1999; Benthien et al., 2002; Pagani et al., 2002).

2.2. Laboratory Methods

All biomarker analyses were conducted at the Lamont-Doherty Earth Observatory of Columbia University (LDEO; New York, USA). All coccolith measurement work was conducted at the Centre Européen de Recherche et d'Enseignement des Géosciences et de l'Environnement (CEREGE; Aix-en-Provence, France). The details of lipid extraction, isotope measurement, and nannofossil slide preparation and coccolith size measurements are described in the Supporting Information S1 and are briefly summarized here.

Sediment samples were freeze dried and free lipids were extracted using a DIONEX ASE 350. Alkenones were purified from the total lipid extract using small-scale silica gel column chromatography. The dichloromethane fraction containing the alkenones was saponified to remove interfering long-chain fatty-acid methyl esters.

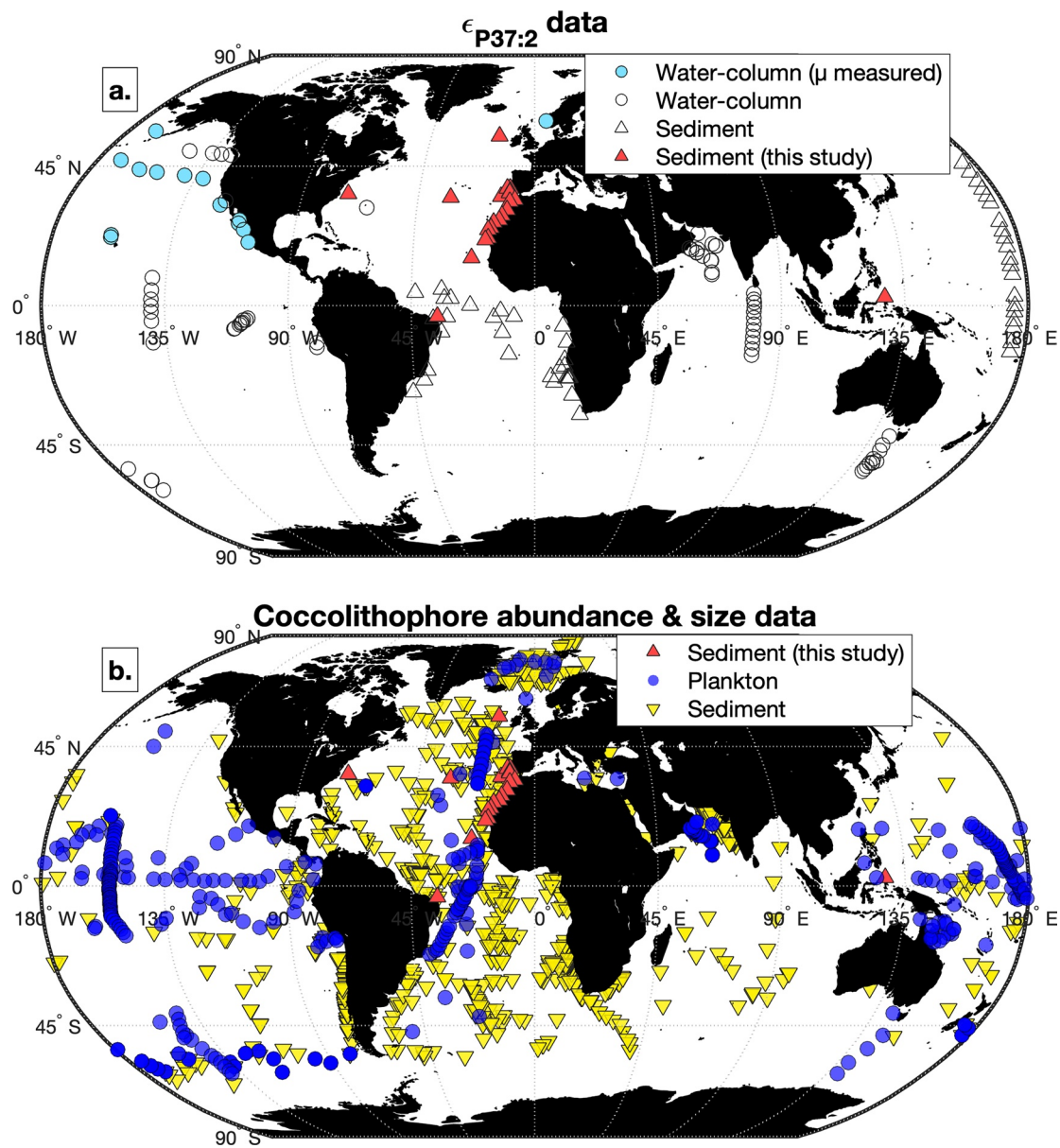


Figure 1. Locations of samples used in this study. (a) Water-column and sediment sample locations for ϵ_p data. Filled aqua circles are “training set” water-column samples where growth rate (μ) was measured in-situ ($n = 108$); filled red triangles are new surface sediments ($n = 22$); open circles and triangles are previously reported water-column ($n = 117$) and surface sediment data ($n = 49$), respectively. (b) Coccolithophore abundance and size data mined from the literature (water-column $n = 803$; sediment $n = 1019$), as well as new sediment samples ($n = 22$; red, same as above).

Alkenone unsaturation ratios were measured by gas chromatography with flame ionization detection, which were converted to temperature using the calibration of Müller et al. (1998). We measured alkenone carbon isotope ratios by gas-chromatograph isotope ratio mass spectrometry (GC-irMS). The average uncertainty was 0.31‰ ($n = 22$), which includes realizing sample delta values on the VPDB scale (Polissar & D’Andrea, 2014).

Coccolith size measurements were made by automated microscopic imaging coupled to coccolith identification and morphometric analysis using the SYRACO software program (Barbarin, 2014; Beaufort & Dollfus, 2004). Details regarding the microscope set-up and imaging can be found in Beaufort et al. (2020) and are summarized in the Supporting Information S1. Briefly, bulk sediment was sieved at 25 μm in deionized water alkalinized to pH ~ 9 with dilute ammonium hydroxide. At least two coverslips for each sample were prepared by random settling of the <25 μm fraction. On a Leica DM6000 polarizing microscope equipped with bidirectional circular

polarization, we imaged between 165 and 297 fields of view of each coverslip using a grayscale SPOTFLEX camera (Diagnostic Instruments). For each image, carbonate particles were segmented from the black background, and nanofossils were identified and classified into 33 different groups—separated roughly at the genus or family level—using a machine-learning-based software program (SYRACO) that was trained to identify Cenozoic coccoliths (Barbarin, 2014). Morphometric parameters, such as coccolith length, were determined by SYRACO. We manually vetted all coccolith images that were programmatically identified to ensure that coccoliths were properly classified, and to remove misclassified coccoliths from the final data.

2.3. Oceanographic Data

Relevant oceanographic data for this analysis include temperature, salinity, nutrients, $[\text{CO}_{2(\text{aq})}]$, mixed layer depth, surface irradiance (photosynthetically available radiation, PAR), and the diffuse attenuation coefficient of PAR ($K_{d_{490}}$). In cases where temperature, salinity and nutrient information were not reported in the original publication or primary cruise documents, we estimate these parameters from the World Ocean Atlas 2018 gridded climatologies (Garcia et al., 2019a, 2019b; Locarnini et al., 2019) using the interp2 and interp3 functions in MATLAB R2020a with scatteredInterpolant interpolation. For samples with an exact collection date reported, we linearly interpolate between monthly climatological averages to the collection day, with day of year as the time axis and assuming the monthly climatology is reported for the middle day of the month. For sediment samples, we use the annual mean of the monthly climatologies of each oceanographic parameter. While there can be seasonality of algal production, this signal is greatly attenuated by concomitant enhanced remineralization in the subsurface such that alkenone distributions in deep ocean particulate fluxes and surface sediments more closely track mean annual conditions (Rosell-Mel  & Prahl, 2013). Globally, core-top alkenone unsaturation ratios are strongly correlated with mean annual temperatures in the surface ocean (Conte et al., 2006; Kienast et al., 2012; M ller et al., 1998; Sikes et al., 1991, 1997; Sonzogni et al., 1997). Based on the overwhelming mean annual signal, we assume all sediment samples represent mean annual conditions. The majority of our samples come from the low- and mid-latitudes, where this assumption is well-founded (Tierney & Tingley, 2018).

Where not reported, we estimate the depth of the mixed layer at each sample location using the gridded data set of de Boyer Mont gut et al. (2004) with their fixed-threshold temperature criterion, which determines the base of the mixed layer as the depth of a 0.2 C change from the temperature at 10 m depth. This method therefore assumes the minimum mixed layer depth is 10 m, because the upper few meters of the surface ocean are generally subject to significant daily density variations (Schneider & M ller, 1990).

2.3.1. Irradiance

We calculated irradiance over a 24-hr period at the collection (water-column) or production (sediment) depth by:

$$\text{PAR}_z = \text{PAR}_{\text{surface}} \times e^{-K_{d_{490}} \times z} \quad (2)$$

where z = depth (meters, m), $\text{PAR}_{\text{surface}}$ is the incident photosynthetically available radiation at the ocean surface ($\text{mol photons m}^{-2} \text{ d}^{-1}$), and $K_{d_{490}}$ is the diffuse attenuation coefficient of light at 490 nm (m^{-1}) (Falkowski & Raven, 2007). Surface irradiance and $K_{d_{490}}$ at each location were obtained by averaging NASA SeaWiFS and MODIS Aqua data (NASA Goddard Space Flight Center, Ocean Biology Processing Group, 2018a, 2018b, 2018c, 2018d), point-extracted using the interp2 function in MATLAB R2020a with scatteredInterpolant interpolation.

We calculated the hours of daylight at each collection location and date following the equations outlined in the NOAA Sunrise/Sunset and Solar Position Calculators (<https://www.esrl.noaa.gov/gmd/grad/solcalc/calcdetails.html>). As stated in Section 2.3, we assume all sediment alkenone $\delta^{13}\text{C}$ values reflect mean annual production, and employ a photoperiod of 12 hr for all sediment samples.

2.3.2. The Carbonate System, $[\text{CO}_{2(\text{aq})}]$, and $\delta^{13}\text{C}_{\text{DIC}}$

In the water-column samples, all studies (except Schulte et al., 2003 and Gould et al., 2019) determined $[\text{CO}_{2(\text{aq})}]$ during sampling, typically through simultaneous measurement of DIC and total alkalinity. For sediment samples, we must estimate the preindustrial surface ocean $[\text{CO}_{2(\text{aq})}]$. We do this by assuming surface ocean mean annual alkalinity has remained constant over the last several thousand years, and speciate the carbonate system with estimated preindustrial total CO_2 (PI_TCO_2) from the GLODAPv2.2016b mapped climatology (Key et al., 2015; Olsen et al., 2016). We use the CO2SYS MATLAB program (Van Heuven et al., 2011) to speciate the carbonate

system, using the K_1 and K_2 constants of (Lueker et al., 2000), K_{SO_4} of Dickson (1990), and total boron of Uppström (1974).

Determining alkenone ϵ_p ($\epsilon_{\text{p}37:2}$) requires carbon isotope measurements of the $\text{C}_{37:2}$ methyl ketone ($\delta^{13}\text{C}_{\text{MK}37:2}$), the carbon isotope ratio of dissolved inorganic carbon in the ambient seawater ($\delta^{13}\text{C}_{\text{DIC}}$), and temperature, to calculate the carbon isotope ratio of dissolved CO_2 ($\delta^{13}\text{C}_{\text{CO}_2\text{aq}}$). For water-column samples, we use the $\delta^{13}\text{C}_{\text{DIC}}$ measured at the time of sample collection. For sediment samples, we must estimate the pre-industrial surface ocean $\delta^{13}\text{C}_{\text{DIC}}$. Because anthropogenic CO_2 has been preferentially adding $^{12}\text{CO}_2$ to the ocean since the industrial revolution (Keeling, 1979), we cannot use modern values. Instead, we use the GLODAPv2.2019 bottle data set to first estimate modern $\delta^{13}\text{C}_{\text{DIC}}$ values at each sample location (Olsen et al., 2019). We then estimate the anthropogenic contribution to $\delta^{13}\text{C}_{\text{DIC}}$ using the gridded output of the isotope enabled biogeochemical model of Schmittner et al. (2013), which modeled the anthropogenic contribution to $\delta^{13}\text{C}_{\text{DIC}}$ throughout the global ocean. We subtract the $\delta^{13}\text{C}_{\text{DIC_ANT}}$ from modern $\delta^{13}\text{C}_{\text{DIC}}$ at each sample location, yielding an estimate of preindustrial $\delta^{13}\text{C}_{\text{DIC}}$ values. We use this method to estimate $\delta^{13}\text{C}_{\text{DIC}}$ and recalculate $\epsilon_{\text{p}37:2}$ for the core-top datasets of Andersen et al. (1999), Benthien et al. (2002) and Pagani et al. (2002), putting all sediment $\epsilon_{\text{p}37:2}$ data in a common framework. We calculate $\delta^{13}\text{C}_{\text{CO}_2\text{aq}}$ using the temperature-dependent fractionation between DIC and $\text{CO}_{2(\text{aq})}$ of Rau et al. (1996) (Equation S2 in Supporting Information S1). We use alkenone-derived temperatures for sediment samples, with no adjustment to preindustrial conditions, because the temperature change since preindustrial ($\sim 0.9^\circ\text{C}$ on average) has a $\sim 0.1\%$ effect on $\delta^{13}\text{C}_{\text{DIC}}$, and is not significant compared to $\epsilon_{\text{p}37:2}$ measurement uncertainties. The recalculated $\epsilon_{\text{p}37:2}$ values are on average -0.78% different from previously published values (Andersen et al., 1999; Benthien et al., 2002; Pagani et al., 2002).

2.3.3. Collection and Alkenone Production Depths

The collection depth of all water-column samples was reported in their original publications. For sediment samples, the effective depth of alkenone export production is unknown. Alkenone-producing coccolithophores are photoautotrophs and fix carbon in the photic zone. Surveys of coccolithophore abundance find *E. huxleyi* and *G. oceanica* in the upper ~ 200 m of the surface ocean, though vertical distributions vary strongly spatially (Beaufort et al., 2008; Boeckel & Baumann, 2008; Hagino et al., 2000; Haidar & Thierstein, 2001; Okada & Honjo, 1973; Poulton et al., 2017). Here we set the production depth as 75% of the mixed layer depth (MLD) at each location. This fractional depth was chosen by quality of fit to the data through testing several possibilities. We use a fractional depth of the mixed layer at each location so as to treat all sediment samples in a consistent manner. This depth is then used to calculate the average irradiance value for a given sediment sample. This choice of production depth is consistent with the very strong correlation between surface ocean temperatures and alkenone unsaturation ratios in surface sediments (Kienast et al., 2012; Müller et al., 1998; Prah et al., 2006; Sikes et al., 1991, 1997; Sonzogni et al., 1997; Tierney & Tingley, 2018), although there is evidence for alkenone production below the mixed layer but within the photic zone (Ohkouchi et al., 1999; Wolhowe et al., 2014). We further discuss the prescribed production depth in Section 3.4.2.

2.4. Carbon Demand Relative to Diffusive CO_2 Supply (τ)

Laboratory cultures have demonstrated that the expression of RubisCO's preference for ^{12}C over ^{13}C decreases as the ratio of cellular carbon demand to $[\text{CO}_{2(\text{aq})}]$ increases (Burkhardt et al., 1999; Laws et al., 1995). A convenient way to describe the ratio of carbon demand to CO_2 supply is the dimensionless unit τ of McClelland et al. (2017):

$$\tau = \frac{r\mu_i}{3P_c C_e} \quad (3)$$

where r is the cell radius (m), μ_i is the photoperiod-adjusted growth rate (Rost et al., 2002), ρ is the cellular carbon density (pmol C m^{-3}), C_e is the ambient $[\text{CO}_{2(\text{aq})}]$ (mol C m^{-3}), P_c is the diffusive cellular permeability to CO_2 (m s^{-1}). This term is equivalent to other demand/supply ratios in the literature (Burkhardt et al., 1999; Popp, Laws, et al., 1998). Blanco-Ameijeiras et al. (2020) measured cell membrane permeability to CO_2 in *E. huxleyi* and found CO_2 permeability was approximately $1\text{e}^{-4} \text{ m s}^{-1}$. However, here we apply an effective permeability of $2.0\text{e}^{-5} \text{ m s}^{-1}$ so τ values used here are comparable to those reported in recent culture work (Phelps et al., 2021). The lower permeability that we use accounts for additional restriction of diffusion by the chloroplast and pyrenoid (see Phelps et al. [2021] for further discussion). We treat permeability as a constant in all of our ensuing analysis;

for a consideration of variable membrane permeability on ϵ_p , see Stoll et al. (2019). A different permeability value expands or compresses the τ axis, but it would not affect the relative positioning of data nor our ϵ_p modeling results.

2.5. Coccolithophore Abundance and Coccolith Size Compilation

Unicellular coccolithophorid algae surround their cell walls with calcium carbonate plates called coccoliths. In the alkenone-producing family Noelaerhabdaceae, coccolith dimensions are well correlated to cell radius (Beuvier et al., 2019; Henderiks & Pagani, 2007; McClelland et al., 2016). Here we generate estimates of alkenone-producer cell size in the global ocean, both from new measurements of coccolith length and a compilation of data from the literature. These data allow us to evaluate the influence of cell size on the spatial variation of $\epsilon_{p37:2}$ in the modern ocean. Our algorithm is described in detail in the Supporting Information S1. Briefly, we compile coccolith size and abundance data from published core-top and water column surveys (Figure 1b) (Andrulleit & Rogalla, 2002; Balestra et al., 2010; Baumann et al., 2000; Bendle et al., 2005; Boeckel, 2003; Boeckel & Baumann, 2004; Boeckel et al., 2006; Bollmann, 1997; Bollmann et al., 2009; Bollmann & Herrle, 2007; Bollmann et al., 2002; CLIMAP Project Members, 1976; Cortés et al., 2001; Findlay & Giraudeau, 2000; Frenz et al., 2005; Geitzenauer et al., 1976; Hagino & Okada, 2006; Haidar & Thierstein, 2001; Herrmann et al., 2012; Horigome et al., 2014; Kinkel et al., 2000; Saavedra-Pellitero & Baumann, 2015; Saavedra-Pellitero et al., 2010, 2014; Schiebel et al., 2004, 2011; Schwab et al., 2012). Using the coccolith size range defining each species as reported by the Nannotax3 database (Young et al., 2017), we estimate a biomass-weighted (“BMW”) coccolith length for the alkenone-producing population at every sample location in Figure 1b. This biomass weighting is necessary because alkenone concentration per cell scales with biomass (Riebesell, Revill, et al., 2000), and biomass is proportional to cube of the radius (Aloisi, 2015; Verity et al., 1992). Therefore, in a population of alkenone-producing coccolithophores, more of the total alkenone production would be sourced by larger cells, and taking the arithmetic mean coccolith size would underestimate the average cell radius that contributed to the $\epsilon_{p37:2}$ signal. We then estimate the average coccolith length at each $\epsilon_{p37:2}$ sample location (Figure 1a) by taking the inverse-distance weighted mean of all coccolith length estimates within 5° of the $\epsilon_{p37:2}$ sample. Finally, we convert coccolith length to cell radius using a linear relationship between cell radius and coccolith length derived from culture data of McClelland et al. (2016) (Equation S5 in Supporting Information S1).

2.6. Noelaerhabdaceae Growth Rate Modeling

We estimate Noelaerhabdaceae growth rates using a modified approach of Krumhardt et al. (2017), referred to henceforth as “K17.” This method models coccolithophore growth rates as a function of temperature and substrate supply. The maximum growth rate is set by a power law of temperature, determined from culture experiments of *Emiliania huxleyi* (Fielding, 2013). The realized growth rate is determined by the growth-limiting parameters following Michaelis-Menten uptake kinetics using published substrate half-saturation (K_M) constants for *Emiliania huxleyi*. We include nitrate, phosphate, CO_2 , and irradiance as growth substrates in our model, while K17 used only CO_2 and phosphate. The equations used to calculate growth rate can be found in the Supporting Information S1 (Equations S7-S10 in Supporting Information S1). We evaluate the skill of this model using a subset of water-column samples where growth rates of alkenone-producing algae were measured either by cell counts (Benthien et al., 2007), or during in-situ incubations by monitoring the uptake of isotopically labeled DIC into alkenones (Prahl et al., 2005; Wallsgrove, 2008; Wolfshorndl et al., 2019; Wolhowe et al., 2014).

2.7. Culture-Based Linear Model of ϵ_p

We model alkenone ϵ_p as a function of $[\text{CO}_{2(\text{aq})}]$ ($\mu\text{mol kg}^{-1}$), total daily irradiance (“PAR,” $\text{mol photons m}^{-2} \text{d}^{-1}$; i.e., irradiance in a 24-hr period), cell radius (“ R_C ,” μm), and growth rate (d^{-1}) after (Phelps et al., 2021).

$$\epsilon_{p37:2} = -8.6e^{-3} \times [\text{CO}_{2(\text{aq})}]^2 + 0.48 \times [\text{CO}_{2(\text{aq})}] + 0.48 \times \text{PAR} - 3.86 \times R_C - 0.26 \times \mu + 13.68 \quad (4)$$

The statistics of the model can be found in the Supporting Information S1. The coefficient on growth rate is so small relative to the range of reasonable growth rates ($\sim 0.1\text{--}1 \text{d}^{-1}$ for the Noelaerhabdaceae) that it has a negligible effect on the modeled ϵ_p values: an increase from 0 to 1d^{-1} has only a -0.26% effect on ϵ_p , which is within

the alkenone $\delta^{13}\text{C}$ measurement uncertainty. We address the parameterization of growth rates in the Supporting Information S1, but we stress that uncertainty in growth rate does not affect the interpretation or application of this culture-based linear model (see Section 3.6).

3. Results and Discussion

Culture studies have shown that irradiance, environmental conditions (e.g., batch or chemostat cultures), and algal carbon demand relative to diffusive CO_2 supply (τ) are important determinants of coccolithophore carbon isotope fractionation, ϵ_p (McClelland et al., 2017; Phelps et al., 2021; Popp, Laws, et al., 1998; Riebesell, Burkhardt, et al., 2000; Rost et al., 2002). Here we examine whether these same factors are primary controls on alkenone ϵ_p in the ocean. First, we use our new results to evaluate for the first time whether there is evidence for a strong effect of cell size on $\epsilon_{p37:2}$ in the modern ocean and in recent sediments, and whether cell size and growth rate are correlated. Next, we evaluate the consistency of $\epsilon_{p37:2}$ variations with traditional models of control by the ratio carbon demand to supply (τ). Subsequently, we consider if irradiance plays a key role in explaining $\epsilon_{p37:2}$ variations in sediments and the water column, as observed in culture experiments. Finally, we contrast a culture-based model that includes irradiance (Phelps et al., 2021) with the diffusive model “b” approach for reconstructing $p\text{CO}_2$ from $\epsilon_{p37:2}$ in sediments, and provide recommendations for paleobarometry.

3.1. Does Noelaerhabdaceae Cell Radius Correlate With Growth Rate or $\epsilon_{p37:2}$?

In our new core-top samples, biomass-weighted (BMW) mean coccolith length ranges from 3.45 to 5.19 μm ($n = 22$, mean = 4.63 $\mu\text{m} \pm 0.47$, 1σ). This size distribution is consistent with a majority of *E. huxleyi* Type A and *G. oceanica* morphotypes, the dominant morphotypes in the low-latitudes, from which the majority of our new samples originate. In this subset, we do not find a statistically significant linear correlation (defined as $p < 0.05$) between BMW mean coccolith size and $\epsilon_{p37:2}$ or temperature, irradiance, or macronutrient concentrations. A weak but significant correlation is found between BMW mean coccolith length and $p\text{CO}_2$ ($r^2 = 0.27$, $p < 0.05$). When we combine our new measurements with size estimates in the full alkenone compilation ($n = 186$, including both core-top and water-column samples), BMW mean coccolith length ranges from 2.56 to 5.19 μm (mean = 3.60 $\mu\text{m} \pm 0.59$, 1σ). Cell radius is a linear translation of coccolith length, and ranges from 1.91 μm to 3.41 μm (mean = 2.50 $\mu\text{m} \pm 0.33$, 1σ). Mean cell radius in sediment samples is 2.74 $\mu\text{m} \pm 0.35$ (1σ), while in water-column samples it is 2.39 $\mu\text{m} \pm 0.26$ (1σ). These are statistically different according to a Kolmogorov-Smirnov test.

There is no statistically significant correlation between BMW coccolith length and estimated growth rate in the combined data set (Figure 2e). This result contrasts with that of Zhang et al. (2020), who found a negative correlation between growth rate and estimated cell volume in *E. huxleyi* grown in chemostat and semi-continuous batch cultures. We elaborate on this discrepancy in the Supporting Information S1, and note that we posit that the relationship in cultures is an artifact of the data treatment and analysis by Zhang et al. (2020); our reanalysis of the culture data set finds no significant relationship between cell size and growth rate (Figure S4; Text 2.2 in Supporting Information S1). In a culture study exploring allometry across nine coccolithophore species, Villiot et al. (2021) also found no relationship between growth rate and cell size within the Noelaerhabdaceae. In the combined data set, we also observe weak but significant inverse correlations between BMW coccolith length and phosphate, nitrate, $p\text{CO}_2$, irradiance, a weak positive correlation between BMW coccolith length and temperature, and no statistically significant correlation between coccolith length and $\epsilon_{p37:2}$ (Figure 2).

In the global alkenone ϵ_p data set we observe both large and small coccolith sizes at low irradiance, but a trend toward smaller coccoliths as irradiance increases ($r^2 = 0.02$, $p < 0.05$). This relationship contrasts with that in planktonic foraminifera, where irradiance is an important driver of larger test sizes (Lombard et al., 2010; Spero & Lea, 1993). In the Noelaerhabdaceae, cell size is closely related to species and morphotype. The observed trends may therefore reflect top down (ecosystem) rather than bottom up (direct resource availability and plastic response) controls. It is possible therefore that Noelaerhabdaceae size is controlled by more complex competitive interactions, particularly in locations with dynamic hydrography. For example, although *E. huxleyi* is the dominant species around the world, different regions are occupied by genetically distinct strains (Iglesias-Rodriguez et al., 2006), thus there may be niche partitioning related to the presence and absence of other phytoplankton

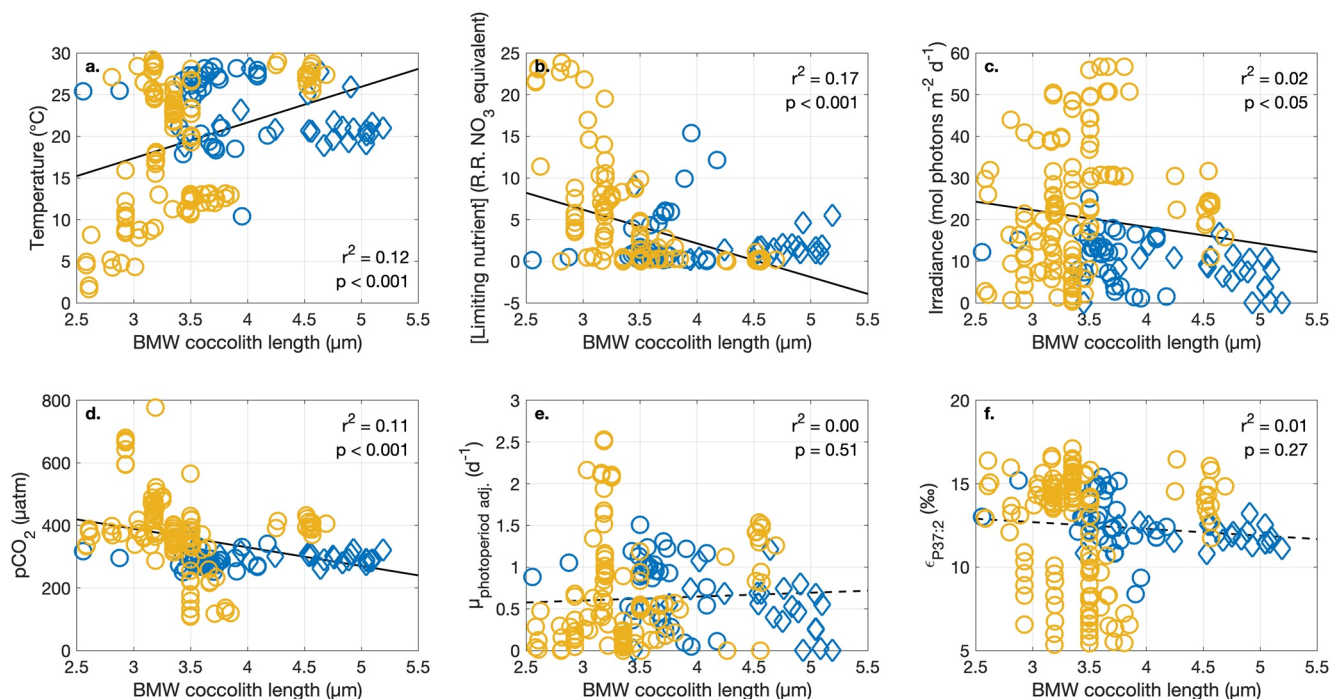


Figure 2. Biomass-weighted coccolith lengths in the alkenone ϵ_p sample set. Linear relationships between biomass-weighted coccolith length and environmental variables for sediment (blue) and water-column (gold) samples. Diamonds represent new sediment samples, circles portray previously reported samples. (a) Temperature; (b) the concentration of the limiting nutrient (N or P) adjusted to nitrate-equivalence by the Redfield ratio; (c) irradiance at the collection or production depth; (d) in-situ $p\text{CO}_2$; (e) photoperiod-adjusted growth rate; (f) $\epsilon_{p37:2}$. In all panels, solid lines show slopes significant at the $p < 0.05$ confidence interval; dashed lines show statistically insignificant correlations.

groups, or micronutrient availability governing which strain or species dominates, neither of which we have the data to test.

3.2. Is Alkenone ϵ_p Related to the Ratio of Cellular Carbon Demand to Diffusive CO_2 Supply?

In our new sediment samples, alkenone ϵ_p ranges from 10.8 to 13.2‰, which is about half the modern sediment range when all data are considered (~8.4–15.4‰). The $\epsilon_{p37:2}$ range in water-column samples is about twice as large as that in sediments (~5.3 to ~20.1‰; Figure 3). The larger variability in water-column $\epsilon_{p37:2}$ likely results from the sampling of depths and environmental conditions that are not equivalent to the average conditions preserved in the sedimentary record. In other words, the sediment samples represent an integration of hundreds to thousands of years of variability, while the water-column samples represent a snapshot of the specific niche and environmental conditions occupying that location at the time of sampling. In the sediment sample set, $[\text{CO}_{2(\text{aq})}]$ ranges from 6.6 to 14.5 $\mu\text{mol kg}^{-1}$, in water-column samples the range is 4.5 $\mu\text{mol kg}^{-1}$ to 32.5 $\mu\text{mol kg}^{-1}$. The higher maximum $[\text{CO}_{2(\text{aq})}]$ results from sampling higher latitude sites with lower temperatures and higher $\text{CO}_{2(\text{aq})}$ solubilities. When the water-column and sediment data are taken together, there is no universal relationship between ϵ_p and $1/[\text{CO}_{2(\text{aq})}]$ (Figures 3a and 3c). Culture observations demonstrate an overall decrease in ϵ_p as $1/[\text{CO}_{2(\text{aq})}]$ increases (Phelps et al., 2021); sediment samples, however, have a positive relationship ($r^2 = 0.05$, $p < 0.1$) with $1/[\text{CO}_{2(\text{aq})}]$ (Figure 3a), an observation first made by Andersen et al. (1999) and reinforced by our new data. The theory underpinning the conventional diffusive alkenone CO_2 proxy requires high ϵ_p values at low $1/[\text{CO}_{2(\text{aq})}]$ values, which is not the case in the sediment data (Figure 3a).

We examine trends in $\epsilon_{p37:2}$ with respect to τ because it is the cellular carbon demand relative to ambient CO_2 supply, rather than CO_2 supply alone, that has been shown to influence ϵ_p in cultures, with lower ϵ_p found at higher τ , and changes in cell size or growth rate could therefore be masking the expected effect of CO_2 (Burkhardt et al., 1999; Laws et al., 1995; McClelland et al., 2017; Popp, Laws, et al., 1998). The τ range in sediments (~0.01–~1.79) is larger than that in water-column samples (0–~1.57), resulting from the combination of low pre-industrial CO_2 concentrations and relatively high modeled growth rates due to high temperatures and high

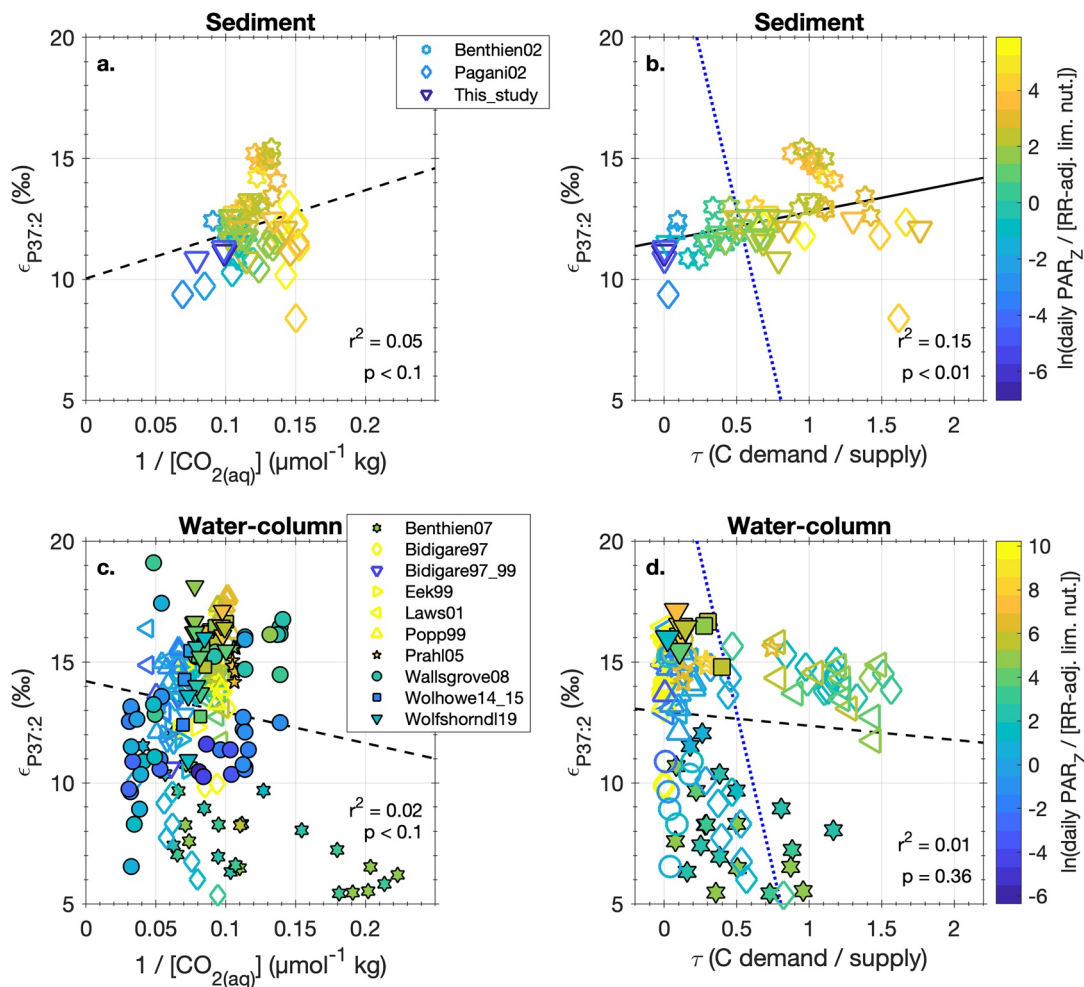


Figure 3. Alkenone carbon isotope discrimination in the natural environment. Carbon isotope ratios in alkenones (ϵ_p) as a function of $1/[CO_{2(aq)}]$ (a), (c) and τ (b), (d), cellular carbon demand divided by $CO_{2(aq)}$ supply. Filled symbols in (c) and (d) are samples with measured growth rates, all others are modeled. There are fewer data in panels (b) and (d) than (a) and (c) because cell size could not be estimated in all samples. Black lines are linear regressions to all data in each panel. In the “sediment” data, six-point stars labeled “Benthien02” also include the data of Andersen et al. (1999), because they were republished by Benthien et al. (2002). Dotted blue lines in (b) and (d) are the diffusive model prediction. Error bars are omitted for clarity; 1σ error on $\epsilon_{p37:2}$ is typically $<0.5\text{‰}$, and is smaller than the size of the symbol. Symbols are colored by the “energy quotient” defined in Equation 5.

irradiance in tropical locations (Figure S1 in Supporting Information S1). This τ range in the natural environment is about 1/3 of the range achieved in *Noelaerhabdaceae* culture experiments (Phelps et al., 2021). Between τ values of 0 and 2 in cultures, ϵ_p spans nearly a 15‰ range, depending on the nutrient and light conditions. This phenomenon is also apparent in water-column samples, with higher irradiance yielding higher $\epsilon_{p37:2}$ at low τ values (Figure 3d). Contrary to primary observations in cultures, $\epsilon_{p37:2}$ increases with increasing τ in sediment samples (Figure 3b; $p < 0.01$).

3.3. Is Alkenone ϵ_p Related to Nutrient and Irradiance Availability?

Phelps et al. (2021) showed from culture experiments of *Noelaerhabdaceae* coccolithophores that the ratio of irradiance to nutrients, in addition to τ , is an important factor controlling ϵ_p . Previous investigators have noted differences between ϵ_p from chemostat cultures and batch cultures of both diatoms and coccolithophores (Pagani, 2014; Riebesell, Burkhardt, et al., 2000), suggesting the interplay of light energy and nutrient availability modulate carbon acquisition and isotope fractionation (Wilkes & Pearson, 2019). Here we calculate an “energy quotient” (Equation 5) as the natural log of integrated daily irradiance (transformed to account for the

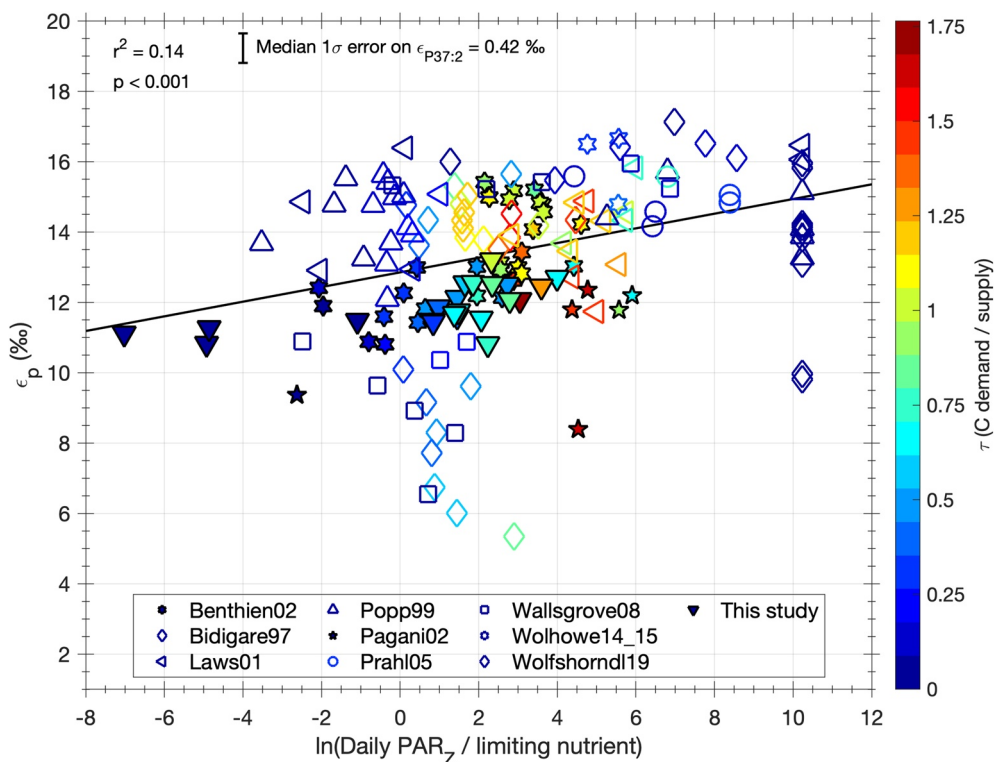


Figure 4. Alkenone ϵ_p as a function of the energy quotient in open ocean water-column and particulate sediment samples. The energy quotient is calculated by taking the natural log of the ratio of daily irradiance at the collection depth to the Redfield ratio-adjusted limiting nutrient concentration. Filled symbols are sediment samples, open symbols are water-column samples, both are colored by τ (C demand/diffusive CO_2 supply). While the ratio of irradiance to nutrients does not explain a majority of the variance in ϵ_p , it is significantly positively correlated with $\epsilon_{p37:2}$ spatially in the modern ocean, as in culture experiments (Phelps et al., 2021). The correlation coefficient and p -value of the regression are calculated using the *fitlm* function in MATLAB R2020a with “robust” fitting to reduce outlier effects.

exponential decay in irradiance from surface to depth) relative to the Redfield ratio-adjusted minimum macronutrient concentration in each sample.

$$\text{energy quotient} = \ln \left(\frac{\text{daily PAR}_z}{\min(\text{PO}_4^{3-} \times 16, \text{NO}_3^-)} \right) \quad (5)$$

Samples with limiting nutrient concentrations below the detection limit (i.e., values of zero) produce infinite energy quotients; we set these values to the maximum of the calculable energy quotient in the data set. When we regress ϵ_p versus this energy quotient (Figure 4), we find a significant relationship in both the water-column and sediment samples, where higher ϵ_p is found at higher irradiance relative to nutrient concentrations ($r^2 = 0.14$, $p < 0.001$). Although this parameter does not explain a majority of the variance in ϵ_p , the finding is in direct agreement with the results from culture data, in which higher integrated irradiance yields higher ϵ_p values (Phelps et al., 2021). A comparison of Figures 3 and 4 suggests that in the natural environment, oceanographic conditions (light and nutrients) are an even more important predictor of ϵ_p than the physiological components encapsulated in τ . There is no universal relationship between $\epsilon_{p37:2}$ and τ in the combined sediment and water-column samples, but there is a similar direction of proportionality in the two sample sets when viewed through the lens of the energy quotient: $\epsilon_{p37:2}$ increases as light relative to nutrients increases.

As discussed in the previous section, we find a positive correlation between $\epsilon_{p37:2}$ and $1/[\text{CO}_{2(\text{aq})}]$ and τ in the sediment samples (Figures 3a and 3b). This is opposite the direction expected if carbon isotope fractionation followed principles of diffusive supply. The absence of the expected relationship likely arises because $[\text{CO}_{2(\text{aq})}]$ and integrated irradiance are significantly inversely correlated (Figure S2 in Supporting Information S1; $r^2 = 0.49$,

$p < 0.001$), and because empirical models from culture data have shown CO_2 and irradiance to have roughly equal but opposite effects on ϵ_p (Phelps et al., 2021). The combination of high irradiance and high $[\text{CO}_{2(\text{aq})}]$ does not exist in the natural environment (Figure S2 in Supporting Information S1). Because of the temperature-dependent solubility of CO_2 , higher $[\text{CO}_{2(\text{aq})}]$ generally occurs at higher latitudes where surface irradiance is generally lower, a result of Earth's tilt and a more oblique angle of incidence for incoming solar rays. The low irradiance at these locations would reduce ϵ_p , compensating for the effect of higher CO_2 . The slope of irradiance versus CO_2 is ~ -3 mol photons $\text{m}^{-2} \text{d}^{-1}$ per $\mu\text{mol kg}^{-1}$, suggesting that the increase in CO_2 as irradiance declines is not sufficient to compensate for the effect of lower irradiance on $\epsilon_{p37.2}$ (Figure S2 in Supporting Information S1).

3.4. Application of a Culture-Based ϵ_p Model to Marine Samples

A recent empirical study by Stoll et al. (2019) demonstrated that Noelaerhabdaceae ϵ_p could be modeled with high accuracy and precision using photoperiod-adjusted growth rate, cell size, $[\text{CO}_{2(\text{aq})}]$, and light intensity. Phelps et al. (2021) updated and modified this multiple linear regression model and used $[\text{CO}_{2(\text{aq})}]$, cell radius, non-photoperiod-adjusted growth rate, and total daily irradiance as predictors, explaining $\sim 70\%$ of the variance in ϵ_p in cultures (Equation 4).

Importantly, the coefficient on μ is negligible: a 1 d^{-1} increase in μ causes only a 0.26% reduction in $\epsilon_{p37.2}$, which is smaller than the typical uncertainty on $\epsilon_{p37.2}$. Because measured growth rates range between 0 and 1 d^{-1} (Figure S1 in Supporting Information S1), growth rates need not be well constrained to apply this model. While both Stoll et al. (2019) and Hernández-Almeida et al. (2020) tested the relationship between modeled and measured $\epsilon_{p37.2}$ in the modern ocean and core-top sediments, our analysis herein differs based on the nuances of the ϵ_p model, the approach to constrain growth rate, updated cell size estimates, and our new $\epsilon_{p37.2}$ data. Below we examine whether the integrated daily irradiance model of Phelps et al. (2021) (Equation 4) is applicable to the natural environment (Figure 5).

3.4.1. Application of a Culture-Based ϵ_p Model to Water-Column Samples

In the water-column data set, using in-situ light, $[\text{CO}_{2(\text{aq})}]$, and estimated cell size and growth rate as inputs into Equation 4, we are unable to model $\epsilon_{p37.2}$ with much precision or accuracy (Figures 5a and 5c). The strong positive correlation between irradiance and model error suggests irradiance is driving much of the model mismatch (Figure 5e). Here we discuss plausible explanations for why the water-column $\epsilon_{p37.2}$ predictions are so scattered. The first group of reasons pertains to the model calibration and the applicability to the ocean. The water-column data set includes many samples with irradiance values far exceeding than those in the culture calibration (max in cultures = $21.6 \text{ mol m}^{-2} \text{d}^{-1}$, max in water-column = $50.4 \text{ mol m}^{-2} \text{d}^{-1}$). Filtering the samples plotted to include only those with irradiance values less than the maximum irradiance in the culture calibration moderately improves the agreement between the culture and water-column error distributions (Figure 5c, dashed line), and removes most of the samples where $\epsilon_{p37.2}$ is vastly overpredicted. It is also possible that the coefficient on integrated irradiance developed from the culture data may be too large for the ocean or that non-linearities exist at higher irradiance values, leading to an overprediction of $\epsilon_{p37.2}$ at high light. If the influence of irradiance on $\epsilon_{p37.2}$ diminishes as irradiance continues to increase beyond the calibration range, the linear coefficient applied here would overestimate $\epsilon_{p37.2}$. Additional culture work testing the effects of irradiance on $\epsilon_{p37.2}$ and exceeding the current calibration range will be critical for improving our quantitative understanding of the influence of light. We also speculate that it may be possible that Noelaerhabdaceae in the surface ocean respond to high light intensity by increasing calcification and self-shading, effectively reducing the photon flux for photosynthesis and dampening the irradiance effect on $\epsilon_{p37.2}$. Some culture studies show an increase in calcification per cell with increasing irradiance (Rost et al., 2002; Zhang et al., 2015); if active, this phenomenon would lead to an over prediction of $\epsilon_{p37.2}$ in near-surface, high-light samples.

An additional possibility is that the model we use here is structurally limited and is missing complexity of the environmental behavior of algal carbon concentrating mechanisms (CCMs). Using the available data, Phelps et al. (2021) decomposed ϵ_p variability into irradiance, CO_2 , cell size, and growth rate (we reiterate that growth rate has a negligible effect on $\epsilon_{p37.2}$ in the model used here). While the activity of CCMs as expressed in the culture calibration data set is implicitly included in the multilinear model through the chosen predictors, the variable expression of these CCMs at conditions outside the calibration range, such as those in the high-irradiance surface ocean, is not explicitly resolved. It is thus plausible that the model is not properly accounting for the complexity

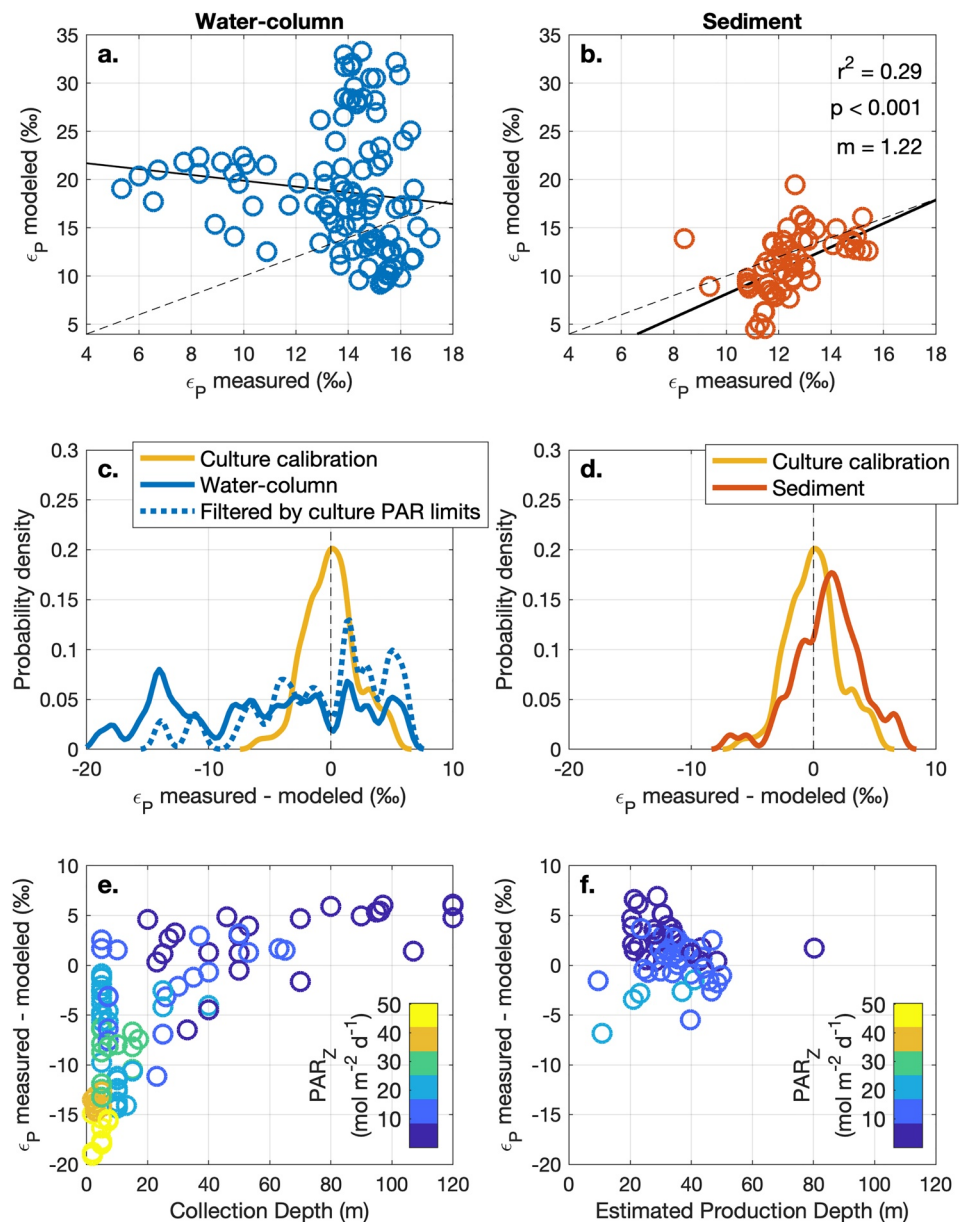


Figure 5. Application of culture-based linear regression model to marine samples. We test the integrated irradiance $\epsilon_{p37:2}$ model (Phelps et al., 2021, Equation 4) on our compiled data set of water-column (a), (c), (e) and sediment (b), (d), (f) samples. (a) and (b): modeled versus measured $\epsilon_{p37:2}$ values in water-columns and sediments, respectively. Dashed line in both panels is the 1:1 line, solid line is a least squares linear regression with the “robust” option in the *fitlm* function. (c) and (d): probability density functions (pdfs, calculated using the *ksdensity* function with a bandwidth of 0.5) of measured minus modeled ϵ_p values from the culture calibration (solid yellow line), water-column (c, blue), and sediment (d, red) samples. Dashed line in (c) shows pdf of measured minus modeled values filtered by the irradiance range in the culture calibration. The close correspondence between the error pdfs of the sediments and cultures demonstrates that the relationships and coefficients derived from culture experiments can be used to predict ϵ_p in surface sediments. (e) and (f): error analysis plotting measured minus modeled $\epsilon_{p37:2}$ values against the collection depth and production depth, respectively; the error in $\epsilon_{p37:2}$ prediction is highly correlated to irradiance in the sample, as shown by the coloring of samples in panels (e) and (f). We exclude the mesocosm data of Benthien et al. (2007) in this analysis because the mixed layer depth values are not equivalent to the rest of the water-column samples.

of CCM activity at the combinations of irradiance and τ in the surface ocean. For example, using a mechanistic model of carbon isotope fractionation in algae, Wilkes and Pearson (2019) proposed a photocatalytic CCM that is upregulated at high irradiance and low nutrient conditions and leads to larger ϵ_p values. This CCM was hypothesized to operate in addition to enhanced bicarbonate uptake stimulated by low CO_2 conditions. Much of the water-column data in our study derive from high irradiance environments. Because the multilinear model we employ here simply requires $\epsilon_{p37.2}$ values increase by 0.47‰ for each additional $\text{mol photons m}^{-2} \text{ d}^{-1}$, it is very likely missing the complexity of CCM behavior, particularly under natural conditions of high irradiance and a light:dark cycle that may induce a fundamentally different physiological response than the 24-hr high light chemostat laboratory experiments used in model calibration. A deeper mechanistic understanding of CCM activity—as well as the presence of the Wilkes and Pearson (2019) photocatalytic CCM—in the natural environment is a target of future work.

The second group of reasons for the water-column $\epsilon_{p37.2}$ mismatch pertains to the environment and our input data. It is possible that the $\epsilon_{p37.2}$ over-prediction results from satellite-derived irradiance values that are too high. Roughly half of the water-column samples in Figure 5 come from ≤ 10 m depth, while the mean mixed-layer depth in these locations is ~ 50 m. Most water-column samples were collected by filtering at the discrete collection depth for less than one day. However, because the upper water column is mixing during sample collection, it is unlikely that the entirety of the biomass collected during sampling was generated under the environmental conditions at that collection depth. It is instead likely that some of the biomass was produced at deeper depths at lower light conditions (giving a lower $\epsilon_{p37.2}$), and mixed upwards to the sampling depth, as alkenone-producing coccolithophores may be concentrated towards the base of the mixed layer in the lower euphotic zone (Beaufort et al., 2008; Poulton et al., 2017; Wolhowe et al., 2014). Gould et al. (2019) presented such an argument in their analysis of water-column alkenone hydrogen isotope data, and reasoned that their water-column samples, which were obtained through hull-mounted seawater pumps, likely included allochthonous alkenones. Algae have a Lagrangian history and the conditions at the depth of collection are not necessarily identical to those at the depth of production, a phenomenon that has also been observed for alkenone unsaturation ratios (cf. Conte et al., 2006; Gould et al., 2017). Furthermore, in the majority of the water-column samples, we estimated irradiance from satellite-based mean monthly climatological datasets because the measurements were not typically made during alkenone sampling. It is entirely possible that the days surrounding alkenone sampling were more or less cloudy, or the water column more or less turbid, than the mean monthly values estimated from satellite-based mission composite climatologies. Divergence from the monthly mean values could lead to higher or lower light intensity when the alkenones in the water-column sample were produced, ultimately resulting in greater mismatch between the measured and modeled $\epsilon_{p37.2}$ values. As a way to explore the data and model assuming perfect parameterization and model fidelity, we solve for the irradiance needed to match $\epsilon_{p37.2}$ (Figure S3 in Supporting Information S1). For $\sim 75\%$ of the water-column samples, the solved irradiance is much lower than the prescribed irradiance at the sampling depth. This suggests that a large portion of the alkenones collected during water column sampling may have been produced under lower light conditions, at deeper depths in the mixed layer, and mixed up to the collection depth. We caution that this analysis requires some samples have negative irradiance values to produce the low $\epsilon_{p37.2}$ values observed, which we attribute to the noisiness of the system. Nevertheless, for $\sim 80\%$ of the non-negative samples, the solved production depths are deeper than the collection depth but still within the mixed layer, suggesting incorporation of alkenones produced under lower-light conditions is possible.

The water-column data set is also shaped by the nature of shipboard sampling and potential oceanographic environments. For example, more than 50% of the water-column samples for which $\epsilon_{p37.2}$ could be modeled were collected at 5 m depth (median = 10 m, $1\sigma = 30.2$ m; Figure S8a in Supporting Information S1); mixed layer depths in this sample set are much deeper (median = 45.9, $1\sigma = 27.3$ m). Because irradiance is attenuated exponentially with depth (Equation 2), this results in a skewed distribution with irradiance biased to surface conditions. This is further evident when collection depths are viewed as a fraction of mixed layer depth at each location (Figure S8b in Supporting Information S1). The majority of samples were collected from the upper $\sim 25\%$ of the mixed layer. While a handful of depth profiles have been collected, shallow, high-irradiance conditions are over-represented.

3.4.2. Application of a Culture-Based ϵ_p Model to Sediment Samples

In contrast to the water-column samples, the culture-based model (Equation 4) performs much better predicting $\epsilon_{p37.2}$ in sediment samples (Figures 5b and 5d). With reasonable estimates of preindustrial $[\text{CO}_{2(\text{aq})}]$, cell radius from coccolith length, and measured $\epsilon_{p37.2}$, the only significant free parameter in the model is irradiance. At

each location, there is an irradiance value that would model $\epsilon_{p37:2}$ in perfect agreement with the measured value. However, here we want to test the global continuity of the $\epsilon_{p37:2}$ response, and therefore must treat irradiance in a consistent manner across the data set. As described in Section 2.3.3, we set the depth of production as 75% of the mixed layer depth at each core location and calculate the irradiance at that depth. This fraction of the mixed layer was chosen empirically: it provided the best fit with the measured $\epsilon_{p37:2}$ data. In sediment samples, mixed-layer depths range from 12.8 to 107 m, with a median of 45.8 m; the average prescribed production depth for sediment samples is 34.8 m ($1\sigma = 10.7$ m, $n = 57$). The average integrated depth of production is therefore towards the base of the mixed layer, where irradiance is lower than at the surface. The correspondence between modeled and measured $\epsilon_{p37:2}$ values in sediment samples (Figure 5b) therefore predicts that the effective average export production depth is $\sim 75\%$ of the mixed layer depth, notably where light-dependent CCMs may be less active. This predicted integrated export depth has implications for models of alkenone fluxes and could be useful in understanding both future and past changes in alkenone export and primary productivity (e.g., Raja & Rosell-Mel , 2021). We note that this is indeed a coarse approximation of alkenone production, but agrees generally with observations of Noelaerhabdaceae habitat (e.g., Okada & Honjo, 1973; Poulton et al., 2017).

With this common fractional depth of production, we are able to grossly model $\epsilon_{p37:2}$ in sediment samples (Figures 5b and 5d). The distribution of measured-modeled values in the sediment sample set is quite similar to that in the cultures (Figure 5d), which further suggests that the same factors controlling alkenone carbon isotope fractionation in cultures are at play in the ocean with similar quantitative scaling, as indicated by a slope close to one on the measured versus modeled plot in the sediment samples (Figure 5b). This suggests that the multiple linear regression is able to quantitatively extract information about the controls on ϵ_p in the natural environment. When we take a more restrictive approach to size estimates and limit the merging distance to $\leq 0.5^\circ$, the result holds (Figure S7 in Supporting Information S1). In contrast to the failure in water-column samples, this is likely because the depth-integrated irradiance signal that is incorporated into the sediment reflects production at lower mean irradiance than the surface water-column sampling. Figure 5f supports this argument, as there is a much weaker correlation between prediction error and irradiance in the sediment samples than water-column samples. Because the sediment samples integrate hundreds to thousands of years of alkenone production (10^3 to 10^7 generations of Noelaerhabdaceae), the ability to model $\epsilon_{p37:2}$ with a consistent irradiance treatment across all samples supports the use of this culture-based model as a paleobarometer in ancient sediments.

3.5. Is the Traditional Diffusive Model Supported by Field Data?

3.5.1. Origins of the b Value

The majority of alkenone-based $p\text{CO}_2$ estimates have used a quantitative relationship between $\epsilon_{p37:2}$ and CO_2 that assumes the alkenone-producing algae acquire CO_2 exclusively *via* diffusion (e.g., Jasper & Hayes, 1990; Pagani et al., 1999; Zhang et al., 2019). In its simplest form, the theory underpinning the alkenone paleobarometer derives from models of plants (Farquhar et al., 1982), in which ϵ_p is described by the balance of two fractionating steps: diffusion of CO_2 into the cell ($\sim -0.7\text{‰}$ in solution), and carboxylation by RubisCO ($\sim -25\text{‰}$). The ratio of the cellular carbon fixation rate to the diffusive CO_2 supply rate (a function of the ambient $[\text{CO}_{2(\text{aq})}]$ and the cell membrane surface area and permeability) defines the line between these two fractionating steps, assuming that the rate constants for diffusion into and out of the cell are equivalent. Surveys of bulk marine $\delta^{13}\text{C}_{\text{POC}}$ indeed found an inverse relationship between $\delta^{13}\text{C}_{\text{POC}}$ and CO_2 (Francois et al., 1993; Rau et al., 1989, 1992), as is expected from this theory. Considerations of growth rate, cell size, and active carbon uptake identified that the relationship between ϵ_p and $[\text{CO}_{2(\text{aq})}]$ was modified by physiology. To circumvent the difficulty reconstructing the physiology of alkenone producers through time, $\epsilon_{p37:2}$ is related to $[\text{CO}_{2(\text{aq})}]$ in practice using the empirical relationship:

$$\epsilon_{p37:2} = \epsilon_f - b/[\text{CO}_{2(\text{aq})}] \quad (6)$$

where ϵ_f is the fractionation by RubisCO ($\sim 25\text{‰}$), and the b term accounts for all non- CO_2 effects on ϵ_p (Bidigare et al., 1997; Jasper et al., 1994). This equation was introduced by Jasper et al. (1994) and has been the primary approach for alkenone paleobarometry for over two decades (Pagani et al., 1999; Zhang et al., 2020). A mechanistic model by Rau et al. (1996) demonstrated that in this model, b is directly proportional to growth rate and cell radius, a finding that seemed confirmed by a linear relationship between ϵ_p and μ/CO_2 in nitrate-limited chemostat cultures of *E. huxleyi* grown under high and continuous irradiance conditions (Bidigare et al., 1997).

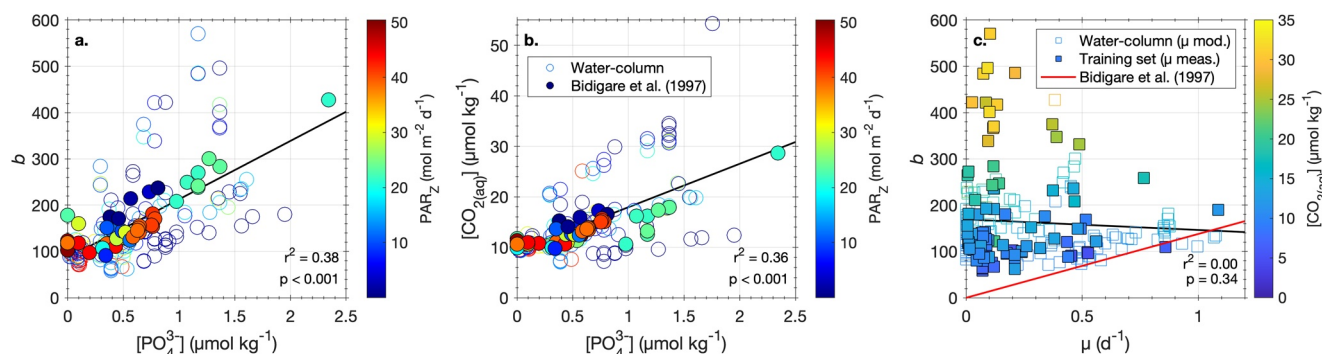


Figure 6. Assessment of the conventional diffusive alkenone- $p\text{CO}_2$ proxy. (a) b value calculated using Equation 6 as a function of in-situ $[\text{PO}_4^{3-}]$. In (a) and (b), filled symbols are the data used by Bidigare et al. (1997) for the b value calibration from water-column samples; open symbols are all data generated from open-ocean water-column samples since 1997. (b) In-situ aqueous CO_2 concentrations regressed against phosphate concentrations. (c) b plotted against cellular growth rate; filled symbols are samples with measured growth rates in the field, open symbols are samples where growth rate is modeled; samples are colored by $[\text{CO}_{2(\text{aq})}]$. The conventional alkenone- $p\text{CO}_2$ proxy (diffusive model) argues that b and μ are directly proportional (red line in panel c), but existing data show the opposite relationship.

Because growth rates have been difficult to estimate by proxy, empirical calibrations from modern water-column samples (a subset of the “water-column” data set presented here) related b to in-situ $[\text{PO}_4^{3-}]$, which were found to be very highly correlated in the original calibration set ($r^2 = 0.95$, Bidigare et al., 1997). In applied paleobarometry, the b value is estimated using modern or modeled $[\text{PO}_4^{3-}]$ at the core location and used to solve Equation 6 for $[\text{CO}_{2(\text{aq})}]$ with the measured $\epsilon_{\text{p37:2}}$. However, this approach has yielded inconsistent results in Pleistocene studies where CO_2 variations are known from ice-core records (Badger et al., 2019; Zhang et al., 2019), and fails to describe $\epsilon_{\text{p37:2}}$ in culture experiments (Hernández-Almeida et al., 2020; Stoll et al., 2019). Here we revisit the statistical and theoretical basis for the conventional alkenone- $p\text{CO}_2$ proxy and argue that it should no longer be used to generate CO_2 reconstructions.

3.5.2. b Reflects $[\text{CO}_{2(\text{aq})}]$, Not Phosphate-Controlled Growth Rate

The original rationale for predicting b from phosphate concentrations was that it had additional explanatory power over CO_2 alone. b is calculated as $b = \text{CO}_2 \times (\epsilon_f - \epsilon_p)$, and any variable that is used to predict b should also be correlated with CO_2 and $(\epsilon_f - \epsilon_p)$. Because b is solved from Equation 6 using water-column samples and in-situ $[\text{CO}_{2(\text{aq})}]$, a correlation between b and $[\text{PO}_4^{3-}]$ could arise from an underlying correlation between $[\text{CO}_{2(\text{aq})}]$ and $[\text{PO}_4^{3-}]$. Bidigare et al. (1997) considered this possibility, and concluded that $[\text{PO}_4^{3-}]$ contained information about b in addition to the minor influence of CO_2 because the correlation between b and $[\text{PO}_4^{3-}]$ ($r^2 = 0.95$) in their calibration data set was much greater than the correlation coefficient between CO_2 and $[\text{PO}_4^{3-}]$ ($r^2 = 0.65$). These authors ascribed this higher correlation to a likely relationship between $[\text{PO}_4^{3-}]$ and growth rate and a dependence of b on growth rate in the diffusive model.

We find the relationship between $[\text{PO}_4^{3-}]$ and b less robust than previously demonstrated (Figure 6a), and $[\text{CO}_{2(\text{aq})}]$ and $[\text{PO}_4^{3-}]$ are about as well correlated as b and $[\text{PO}_4^{3-}]$ ($r^2 = 0.36$ vs. $r^2 = 0.38$, respectively, Figures 6a and 6b). Our analysis suggests $[\text{PO}_4^{3-}]$ does not contain substantial explanatory power for predicting $\epsilon_{\text{p37:2}}$, and the b value is effectively calibrated to $[\text{CO}_{2(\text{aq})}]$. Any apparent success reconstructing past CO_2 with the diffusive model results from the construction of the b parameter and the correlation between near-surface $[\text{PO}_4^{3-}]$ and $[\text{CO}_{2(\text{aq})}]$. For example, Pagani et al. (2002) aimed to test the alkenone- $p\text{CO}_2$ proxy with core-top samples. However, the $[\text{PO}_4^{3-}]$ and $[\text{CO}_{2(\text{aq})}]$ values at the core sites used by Pagani et al. (2002) fall very close to the calibration regression line of Bidigare et al. (1997). If the $[\text{PO}_4^{3-}]$ and $[\text{CO}_{2(\text{aq})}]$ at a core site fall on the calibration relationship, then the mean $[\text{CO}_{2(\text{aq})}]$ reconstructed using $\epsilon_{\text{p37:2}}$ and Equation 6 will as well, because b is solved from $[\text{CO}_{2(\text{aq})}]$ and $\epsilon_{\text{p37:2}}$ in the calibration, and $[\text{PO}_4^{3-}]$ is directly translatable to $[\text{CO}_{2(\text{aq})}]$. Therefore, the measured $\epsilon_{\text{p37:2}}$ values are scaled by b values that were statistically determined to yield the correct modern $[\text{CO}_{2(\text{aq})}]$ by the algebraic formulation of Equation 6. Any study of core-top/modern samples that uses a match between modern and reconstructed CO_2 values as a test of success of the diffusive model will yield a false-positive result because the statistical relationship between ϵ_p , $[\text{PO}_4^{3-}]$ and $[\text{CO}_{2(\text{aq})}]$ is algebraically included in the determination of b .

Bidigare et al. (1997) argued that b , and by correlation, $[\text{PO}_4^{3-}]$, is directly proportional to algal growth rate. This reasoning was supported by evidence available at the time from 24-hr light, nitrate-limited chemostat cultures

with *E. huxleyi*, which yielded a linear relationship between ϵ_p and μ/CO_2 (Bidigare et al., 1997). Additional batch culture experiments with light:dark cycles have since shown that the slope between ϵ_p and τ (proportional to $\mu/\text{CO}_2 \times V/\text{SA}$) is dependent on the τ range of the treatment, and there is in fact a non-linear relationship between ϵ_p and τ (Burkhardt et al., 1999; Laws et al., 2002; Phelps et al., 2021; Wilkes & Pearson, 2019; Stoll et al., 2019). Using published field data where growth rates were measured, we can test whether b is proportional to growth rate. Figure 6c shows relationships between b and μ for samples in our growth rate training set (where growth rates were measured using in-situ isotope-labeling incubations or cell counts), as well as the entire water-column data set (where growth rates are modeled using the modified K17 model; see Supporting Information S1 for details). If the conventional diffusive model accurately and universally described alkenone carbon isotope fractionation in the modern ocean, we would see a positive correlation between b and μ . Instead, we observe the opposite: a wide range of b values are found at low growth rates, but small b values are found at high growth rates (Figure 6c). This is because the highest growth rates occur at high light, high temperature, near-surface locations, where $[\text{CO}_{2(\text{aq})}]$ and $[\text{PO}_4^{3-}]$ are low, but $\epsilon_{p37:2}$ is high as a result of high irradiance. Arithmetically, these combine in Equation 6 to produce a low b value. Hernández-Almeida et al. (2020) probed the relationships between b and other environmental variables, and came to a similar conclusion that b is correlated to $[\text{CO}_{2(\text{aq})}]$ and $[\text{PO}_4^{3-}]$ in the field. In an analysis of b in culture experiments, these authors also found that it is not possible to predict b with any confidence from growth rate, cell size, or light, and that the proposed dependence of b on growth rate is not found in well-controlled culture experiments. The theoretical underpinnings of the conventional alkenone- $p\text{CO}_2$ proxy and the formulation of b are therefore not supported when the entirety of the existing calibration data are considered.

One could argue that the relationship between ϵ_p and $[\text{CO}_{2(\text{aq})}]$ through b is simply empirical, and all non- CO_2 effects—including but not limited to cell size, growth rate, carbon concentrating mechanisms, and irradiance—are encapsulated in b . While that is mathematically true, there is no immediately apparent way to quantitatively scale b for changes in these non- CO_2 effects. Because the theory behind the CO_2 -diffusion model does not accurately describe photosynthetic carbon isotope fractionation in these algae, attempts to modify b for changes in cell size (Henderiks & Pagani, 2007, 2008; Rau et al., 1996; Zhang et al., 2020) have limited quantitative basis when the full culture and modern datasets are considered. Therefore, b , as originally designed and as subsequently modified, is not supported by the breadth of culture or modern ocean data and should not be used for alkenone paleobarometry.

3.6. Recommendations for Paleobarometry and the Sensitivity of Alkenone ϵ_p to CO_2 Change

Our ultimate goal is to extract paleoenvironmental information from the carbon isotope signature recorded in alkenone biomarkers. Culture experiments demonstrate that cell size, irradiance, and $[\text{CO}_{2(\text{aq})}]$ are key determinants of ϵ_p (Bidigare et al., 1997; McClelland et al., 2017; Phelps et al., 2021; Popp, Laws, et al., 1998; Riebesell, Revill, et al., 2000; Rost et al., 2002; Stoll et al., 2019). Our analysis of sediment samples (Figure 5d) suggests these same factors are also controlling alkenone carbon isotope fractionation in the natural environment with similar quantitative scaling, providing a framework for interpreting $\epsilon_{p37:2}$ in sedimentary records.

To illustrate the approach, we model $\epsilon_{p37:2}$ at a hypothetical site (5°N, 145°E) in the western Pacific warm pool—an area largely in CO_2 equilibrium with the atmosphere (Takahashi et al., 2014)—for three times in the past, and calculate how changes in CO_2 and other model parameters would manifest in $\epsilon_{p37:2}$ (Figure 7). We prescribe atmospheric CO_2 levels of 180, 280, and 400 ppm for the Last Glacial Maximum (LGM), Holocene, and warm mid-Pliocene, with assumed sea surface temperatures of 26°C, 28°C, and 30°C, respectively. We estimate in-situ $[\text{CO}_{2(\text{aq})}]$ using Henry's Law (Weiss, 1974) assuming a salinity of 35 (typical pelagic surface salinity, though we note salinity has a negligible influence on CO_2 solubility for typical marine conditions). We treat our down-core $\epsilon_{p37:2}$ modeling the same way as a core-top sediment sample. From $\Delta[\text{CO}_{2(\text{aq})}]$ alone, we calculate an $\epsilon_{p37:2}$ change of -0.79‰ from Holocene to LGM, and of $+0.84\text{‰}$ from Holocene to Pliocene (Figure 7a). We note that these changes are small relative to the precision of the $\epsilon_{p37:2}$ measurement (median 1σ uncertainty in the compiled data set is 0.42‰).

We model changes in coccolith length of $\pm 0.75\ \mu\text{m}$, irradiance changes of $\pm 25\%$, and growth rate changes of $\pm 50\%$ and examine the resulting $\epsilon_{p37:2}$. The modeled $\epsilon_{p37:2}$ is very insensitive to growth rate (Figure 7c), which demonstrates that growth rate does not need to be well constrained to interpret past $\epsilon_{p37:2}$ changes. Cell radius (inferred from coccolith length) and irradiance both have strong effects on $\epsilon_{p37:2}$ and will need to be considered

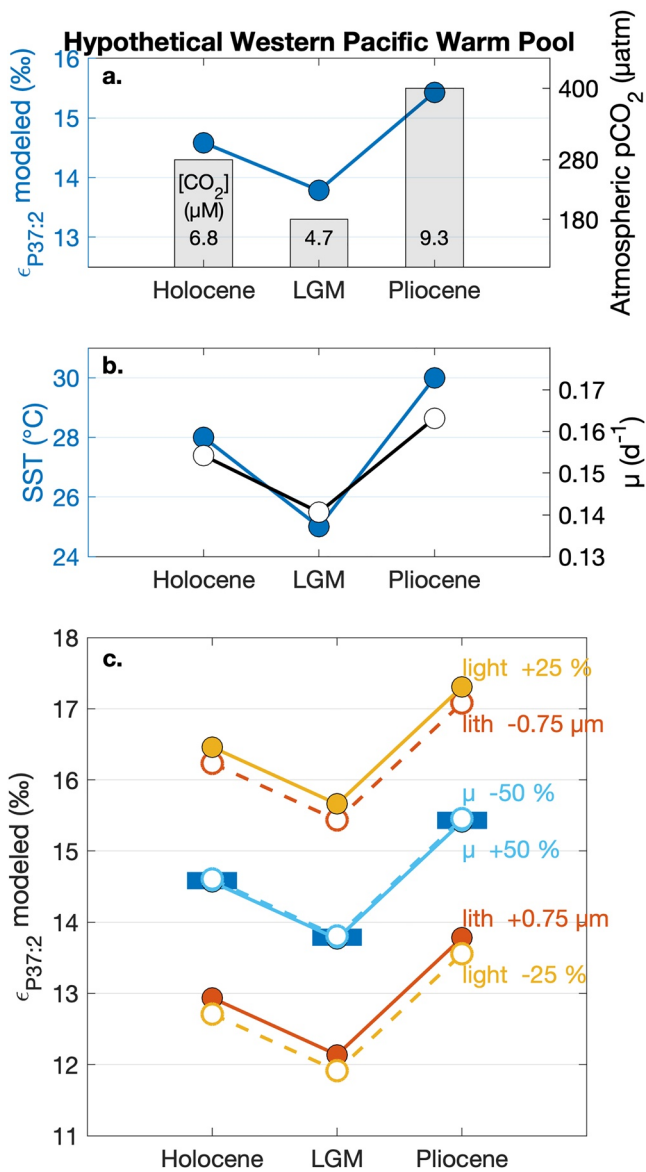


Figure 7. Modeled alkenone ϵ_p in the Pliocene/Pleistocene at a hypothetical location in the Western Pacific Warm Pool. (a) In-situ $[\text{CO}_{2(\text{aq})}]$ for the Holocene, LGM, and Pliocene (3.2–3.8 Ma), from prescribed atmospheric CO_2 concentrations of 280, 180, and 400 ppm, respectively (gray bars; right axis); and modeled $\epsilon_{p37:2}$ resulting from $[\text{CO}_{2(\text{aq})}]$ variations alone (blue; left axis). Numbers in the gray bars indicate the in-situ $[\text{CO}_{2(\text{aq})}]$ ($\mu\text{mol kg}^{-1}$). Irradiance and mixed-layer depths are determined using the same algorithm as for the surface sediment samples, and alkenone $\epsilon_{p37:2}$ is modeled using the integrated irradiance multilinear model (Equation 4). We use a cell radius of 2.44 μm for our baseline case. (b) Sea surface temperatures (blue) and estimated growth rates (black), modeled using the growth rate model described in the text. $[\text{CO}_{2(\text{aq})}]$ in (A) is calculated using the SSTs shown in (b), and assuming constant salinity of 35. (c) Sensitivity of ϵ_p to changes in model parameters on top of ΔCO_2 : irradiance (yellow), growth rate (light blue), coccolith length (red). Dashed lines and open symbols show a reduction in the model parameter value, while solid lines filled symbols show the effect of an increase in the parameter value. Blue bars show the baseline $\epsilon_{p37:2}$ case with only CO_2 sensitivity. For example, the solid red lines show the effect on $\epsilon_{p37:2}$ of increasing coccolith length by 0.75 μm from the baseline scenario with only CO_2 changes (dark blue).

carefully in any paleobarometry applications. Changes in coccolith length have been reconstructed in many locations through the Miocene and Pliocene; some locations show a drop of $\sim 1.5 \mu\text{m}$ in mean length from Pliocene to Holocene (Badger et al., 2019), and a global reduction in Noelaerhabdaceae size in the late Miocene is well documented (Beaufort, 1992; Bolton et al., 2016; Kameo & Bralower, 2000; Takayama, 1993; Young, 1990), which may explain the apparent rise in $\epsilon_{p37:2}$ from the mid-Miocene to Pliocene (e.g., Pagani et al., 1999, 2000). Changes in irradiance also have a large influence on the modeled $\epsilon_{p37:2}$, with a 25% increase in irradiance ($+4 \text{ mol m}^{-2} \text{ d}^{-1}$) roughly equivalent to a 0.75 μm reduction in coccolith length or a 3 $\mu\text{mol kg}^{-1}$ increase in $[\text{CO}_{2(\text{aq})}]$. Explanations for $\epsilon_{p37:2}$ variations in sedimentary sequences will therefore be non-unique, but CO_2 variations can still be extracted by constraining coccolith size and carefully considering irradiance. Changes in the mean depth of alkenone production that arise from changes in water column structure and nutrient availability may have large impacts on the light intensity felt by the alkenone producers and recorded by $\epsilon_{p37:2}$. The impact of changes in production depth also depends on the local attenuation coefficient, a function of the water column turbidity. Irradiance may be best constrained through quantitative bootstrapping, accounting for variations in insolation, and incorporating information from indirect and direct proxies for changes in mixed layer depth and trophic status. While understanding the temporal variations in the parameters influencing $\epsilon_{p37:2}$ records is the subject of ensuing manuscripts and beyond the scope of the present work, our study provides a quantitative framework for considering their effects on CO_2 reconstructions.

Solving our model equation for $[\text{CO}_{2(\text{aq})}]$ will also depend on the uncertainty in realizing ϵ_p , which is a function of alkenone and foraminifera $\delta^{13}\text{C}$ measurement precision, as well as the uncertainty in translating foraminiferal calcite $\delta^{13}\text{C}$ to $\delta^{13}\text{C}_{\text{DIC}}$. Typical precision in modern and paleo ϵ_p samples is between 0.3 and 0.7‰, substantial when compared to the hypothetical changes during the LGM and Pliocene relative to the Holocene. Increasing the number of sites and samples for each reconstruction should help overcome this issue through cancellation of site-specific or random uncertainties, increasing the confidence in estimated paleo- pCO_2 values. Because irradiance cannot easily be constrained in sediment samples, target locations should be those most likely to have a stable irradiance regime. Such locations are pelagic sites with low intra- and interannual variability in mixed layer depth, surface irradiance, and productivity, as all three of these parameters can modulate the penetration of irradiance in the water column. Warm tropical locations that are hydrographically stable may therefore be best-suited for alkenone paleobarometry, while high-latitude or dynamic oceanographic environments should be avoided. The use of other paleoecological and paleoenvironmental proxies (such as multispecies foraminifera or coccolith $\delta^{18}\text{O}$ measurements, or other biomarker abundances (Hernández-Almeida et al., 2020)) in tandem with $\epsilon_{p37:2}$ may help constrain whether light conditions or trophic status at the core location have changed dramatically through time. Nonetheless, that the regression coefficients derived from culture experiments produce reasonable hypothetical changes in $\epsilon_{p37:2}$ over the Plio/Pleistocene suggests it may be possible to tease apart past variations in $\epsilon_{p37:2}$ in terms of three fundamental influences: irradiance, cell size, and CO_2 . Investigations of $\epsilon_{p37:2}$, cell size, and indicators of production depth/mixed layer depth through time periods

of known atmospheric CO₂ change can provide further validation of our model and may lead to an enhanced understanding of atmospheric CO₂ variations in the Cenozoic.

4. Conclusions

Alkenone carbon isotope fractionation ($\epsilon_{p37:2}$) has a long history of being used as an atmospheric pCO₂ paleobarometer. However, recent culture and sediment studies have called into question the fidelity of the proxy. Culture observations have demonstrated that, in addition to cell size, [CO_{2(aq)}], and growth rate, irradiance is a key parameter driving $\epsilon_{p37:2}$ variability. Based on our compilation of published and new data, we observe a dependence of $\epsilon_{p37:2}$ on irradiance in the modern ocean, in both sediment and water-column samples. With a multiple linear regression model derived from culture experiments, we are not able to model $\epsilon_{p37:2}$ well in water-column samples, likely because the alkenones collected during water-column sampling were synthesized throughout the photic zone/mixed layer, and the irradiance at the depth of sampling is too high compared to the average conditions under which the algae grew. However, we show that $\epsilon_{p37:2}$ can be modeled in marine sediments with reasonable accuracy and precision, successfully demonstrating that quantitative relationships derived in culture experiments can explain alkenone $\epsilon_{p37:2}$ variations in sediments. Using measurements mined from the literature of the growth rates of alkenone producers in nature, we show that the theory underpinning the conventional alkenone-pCO₂ proxy and the b parameter are not supported by the field data. This study presents a framework for beginning to quantitatively interpret alkenone $\epsilon_{p37:2}$ variations in ancient sediments, and the extraction of CO₂ information may be possible if irradiance and cell size can be constrained.

Data Availability Statement

The new data generated for this study are reported in table format as Data Supplements. The data have been archived at the Mendeley data repository as: Phelps, Samuel; Stoll, Heather; Bolton, Clara; Beaufort, Luc; Polis-sar, Pratigya (2021), “Controls on Alkenone Carbon Isotope Fractionation in the Modern Ocean—Supporting Data,” Mendeley Data, V1, doi:10.17632/7yfsv5wyk4.2 (available at <https://data.mendeley.com/datasets/7y-fsv5wyk4/2>). Our study represents a significant amount of synthesis and reanalysis of published data. Individual studies and datasets used are included in the references.

Acknowledgments

We thank the Lamont-Doherty Earth Observatory Core Repository for core-top samples used in this analysis. We thank Angela Dial and Yves Gally for sample and laboratory assistance. We thank the Lamont Climate Center and the G. Unger Vetlesen Foundation for financial support. Samuel R. Phelps acknowledges the NSF Graduate Research Fellowship Program (Grant # DGE-16-44869), the Geological Society of America (Grant # 10374-14), and a Grant-In-Aid of Research from the National Academy of Sciences, administered by Sigma Xi, The Scientific Research Society (Grant ID: G20140315448073). Clara T. Bolton acknowledges the projects INSU CALVE and ANR iMonsoon (ANR-16-CE01-0004-01). This material is based upon research supported by the Chateaubriand Fellowship of the Office for Science & Technology of the Embassy of France in the United State. The authors are not aware of any real or perceived financial or affiliate conflicts of interest. We thank Dr. Branwen Williams for her editorial handling of the manuscript as well as three anonymous reviewers whose comments have greatly strengthened this manuscript.

References

- Aloisi, G. (2015). Covariation of metabolic rates and cell size in coccolithophores. *Biogeosciences*, 12(15), 4665–4692. <https://doi.org/10.5194/bg-12-4665-2015>
- Andersen, N., Müller, P. J., Kirst, G., & Schneider, R. R. (1999). Alkenone $\delta^{13}\text{C}$ as a Proxy for Past PCO₂ in Surface Waters: Results from the Late Quaternary Angola Current. In *Use of Proxies in Paleoceanography* (pp. 469–488): Springer Berlin Heidelberg. https://doi.org/10.1007/978-3-642-58646-0_19
- Andrulleit, H., & Rogalla, U. (2002). Coccolithophores in surface sediments of the Arabian Sea in relation to environmental gradients in surface waters. *Marine Geology*, 186(3–4), 505–526. [https://doi.org/10.1016/S0025-3227\(02\)00312-2](https://doi.org/10.1016/S0025-3227(02)00312-2)
- Badger, M. P. S., Chalk, T. B., Foster, G. L., Bown, P. R., Gibbs, S. J., Sexton, P. F., et al. (2019). Insensitivity of alkenone carbon isotopes to atmospheric CO₂ at low to moderate CO₂ levels. *Climate of the Past*, 15(2), 539–554. <https://doi.org/10.5194/cp-15-539-2019>
- Balestra, B., Ziveri, P., Baumann, K. H., Troelstra, S., & Monechi, S. (2010). Surface water dynamics in the Reykjanes Ridge area during the Holocene as revealed by coccolith assemblages. *Marine Micropaleontology*, 76(1–2), 1–10. <https://doi.org/10.1016/j.marmicro.2010.03.002>
- Barbarin, N. (2014). *La reconnaissance automatisée des nanofossiles calcaires du Cénozoïque*. Aix-Marseille University.
- Baumann, K. H., Andrulleit, H., & Samtleben, C. (2000). Coccolithophores in the Nordic Seas: Comparison of living communities with surface sediment assemblages. *Deep-Sea Research Part II: Topical Studies in Oceanography*, 47(9–11), 1743–1772. [https://doi.org/10.1016/S0967-0645\(00\)00005-9](https://doi.org/10.1016/S0967-0645(00)00005-9)
- Beaufort, L. (1992). Size variations in late Miocene Reticulofenestra and implication for paleoclimatic interpretation. *Memorie di Scienze Geologiche*, 43(January 1992), 339–350.
- Beaufort, L., Couapel, M., Buchet, N., Claustre, H., & Goyet, C. (2008). Calcite production by coccolithophores in the South East Pacific Ocean. *Biogeosciences*, 5(4), 1101–1117. <https://doi.org/10.5194/bg-5-1101-2008>
- Beaufort, L., & Dollfus, D. (2004). Automatic recognition of coccoliths by dynamical neural networks. *Marine Micropaleontology*, 51(1–2), 57–73. <https://doi.org/10.1016/j.marmicro.2003.09.003>
- Beaufort, L., Gally, Y., Suchéras-Marx, B., Ferrand, P., & Duboisset, J. (2020). Technical Note: A universal method for measuring the thickness of microscopic calcite crystals, based on Bidirectional Circular Polarization. *Biogeosciences*, 18(February), 1–16. <https://doi.org/10.5194/bg-2020-28>
- Bendif, E. M., Probert, I., Díaz-Rosas, F., Thomas, D., van den Engh, G., Young, J. R., & von Dassow, P. (2016). Recent reticulate evolution in the ecologically dominant lineage of coccolithophores. *Frontiers in Microbiology*, 7(May). <https://doi.org/10.3389/fmicb.2016.00784>
- Bendle, J., Rosell-Melé, A., & Ziveri, P. (2005). Variability of unusual distributions of alkenones in the surface waters of the Nordic seas. *Paleoceanography*, 20(2), PA2001. <https://doi.org/10.1029/2004PA001025>

- Benthien, A., Andersen, N., Schulte, S., Müller, P. J., Schneider, R. R., & Wefer, G. (2002). Carbon isotopic composition of the $C_{37:2}$ alkenone in core top sediments of the South Atlantic Ocean: Effects of CO_2 and nutrient concentrations. *Global Biogeochemical Cycles*, *16*(1), 12–12. <https://doi.org/10.1029/2001GB001433>
- Benthien, A., Zondervan, I., Engel, A., Hefter, J., Terbrüggen, A., & Riebesell, U. (2007). Carbon isotopic fractionation during a mesocosm bloom experiment dominated by *Emiliana huxleyi*: Effects of CO_2 concentration and primary production. *Geochimica et Cosmochimica Acta*, *71*(6), 1528–1541. <https://doi.org/10.1016/j.gca.2006.12.015>
- Beuvier, T., Probert, I., Beaufort, L., Suchéras-Marx, B., Chushkin, Y., Zontone, F., & Gibaud, A. (2019). X-ray nanotomography of coccolithophores reveals that coccolith mass and segment number correlate with grid size. *Nature Communications*, *10*(1), 751. <https://doi.org/10.1038/s41467-019-08635-x>
- Bidigare, R. R., Fluegge, A., Freeman, K. H., Hanson, K. L., Hayes, J. M., Hollander, D., et al. (1997). Consistent fractionation of ^{13}C in nature and in the laboratory: Growth-rate effects in some haptophyte algae. *Global Biogeochemical Cycles*, *11*(2), 279–292. <https://doi.org/10.1029/96GB03939>
- Bidigare, R. R., Fluegge, A., Freeman, K. H., Hanson, K. L., Hayes, J. M., Hollander, D., et al. (1999). Correction to “Consistent fractionation of ^{13}C in nature and in the laboratory: Growth-rate effects in some haptophyte algae” by R.R. Bidigare et al. *Global Biogeochemical Cycles*, *13*(1), 251–252. <https://doi.org/10.1029/1998gb900011>
- Blanco-Ameijeiras, S., Stoll, H. M., Zhang, H., & Hopkinson, B. M. (2020). Influence of temperature and CO_2 on plasma-membrane permeability to CO_2 and HCO_3^- in the Marine Haptophytes *Emiliana huxleyi* and *Calcidiscus leptoporus* (Prymnesiophyceae). *Journal of Phycology*, *56*, 1283–1294. <https://doi.org/10.1111/jpy.13017>
- Boeckel, B. (2003). *Present and past coccolith assemblages in the South Atlantic: Implications for species ecology, carbonate contribution and palaeoceanographic applicability*. Bremen University.
- Boeckel, B., & Baumann, K.-H. (2004). Distribution of coccoliths in surface sediments of the South-Eastern South Atlantic Ocean: Ecology, preservation and carbonate contribution. *Marine Micropaleontology*, *51*(3–4), 301–320. <https://doi.org/10.1016/j.marmicro.2004.01.001>
- Boeckel, B., & Baumann, K.-H. (2008). Vertical and lateral variations in coccolithophore community structure across the subtropical frontal zone in the South Atlantic Ocean. *Marine Micropaleontology*, *67*(3–4), 255–273. <https://doi.org/10.1016/j.marmicro.2008.01.014>
- Boeckel, B., Baumann, K.-H., Henrich, R., & Kinkel, H. (2006). Coccolith distribution patterns in South Atlantic and Southern Ocean surface sediments in relation to environmental gradients. *Deep Sea Research Part I: Oceanographic Research Papers*, *53*(6), 1073–1099. <https://doi.org/10.1016/j.dsr.2005.11.006>
- Bollmann, J. (1997). Morphology and biogeography of *Gephyrocapsa* coccoliths in Holocene sediments. *Marine Micropaleontology*, *29*(3–4), 319–350. [https://doi.org/10.1016/S0377-8398\(96\)00028-X](https://doi.org/10.1016/S0377-8398(96)00028-X)
- Bollmann, J., Henderiks, J., & Brabec, B. (2002). Global calibration of *Gephyrocapsa* coccolith abundance in Holocene sediments for paleotemperature assessment. *Paleoceanography*, *17*(3), 7–1–7–9. <https://doi.org/10.1029/2001PA000742>
- Bollmann, J., & Herrle, J. O. (2007). Morphological variation of *Emiliana huxleyi* and sea surface salinity. *Earth and Planetary Science Letters*, *255*(3–4), 273–288. <https://doi.org/10.1016/j.epsl.2006.12.029>
- Bollmann, J., Herrle, J. O., Cortés, M. Y., & Fielding, S. R. (2009). The effect of sea water salinity on the morphology of *Emiliana huxleyi* in plankton and sediment samples. *Earth and Planetary Science Letters*, *284*(3–4), 320–328. <https://doi.org/10.1016/j.epsl.2009.05.003>
- Bolton, C. T., Hernández-Sánchez, M. T., Fuertes, M.-Á., González-Lemos, S., Abrevaya, L., Mendez-Vicente, A., et al. (2016). Decrease in coccolithophore calcification and CO_2 since the middle Miocene. *Nature Communications*, *7*(1). <https://doi.org/10.1038/ncomms10284>
- Burkhardt, S., Riebesell, U., & Zondervan, I. (1999). Effects of growth rate, CO_2 concentration, and cell size on the stable carbon isotope fractionation in marine phytoplankton. *Geochimica et Cosmochimica Acta*, *63*(22), 3729–3741. [https://doi.org/10.1016/S0016-7037\(99\)00217-3](https://doi.org/10.1016/S0016-7037(99)00217-3)
- CLIMAP Project Members. (1976). The surface of the ice-age Earth. *Science*, *191*(4232), 1131–1137. <https://doi.org/10.1126/science.191.4232.1131>
- Conte, M. H., Sicre, M.-A., Rühlemann, C., Weber, J. C., Schulte, S., Schulz-Bull, D., & Blanz, T. (2006). Global temperature calibration of the alkenone unsaturation index ($U^{K'_{37}}$) in surface waters and comparison with surface sediments. *Geochemistry, Geophysics, Geosystems*, *7*(2), Q02005. <https://doi.org/10.1029/2005GC001054>
- Cortés, M. Y., Bollmann, J., & Thierstein, H. R. (2001). Coccolithophore ecology at the HOT station ALOHA, Hawaii. *Deep-Sea Research Part II: Topical Studies in Oceanography*, *48*(8–9), 1957–1981. [https://doi.org/10.1016/S0967-0645\(00\)00165-X](https://doi.org/10.1016/S0967-0645(00)00165-X)
- de Boyer Montégut, C., Madec, G., Fischer, A. S., Lazar, A., & Iudicone, D. (2004). Mixed layer depth over the global ocean: An examination of profile data and a profile-based climatology. *Journal of Geophysical Research*, *109*(C12), C12003. <https://doi.org/10.1029/2004JC002378>
- Dickson, A. G. (1990). Thermodynamics of the dissociation of boric acid in potassium chloride solutions from 273.15 to 318.15 K. *Journal of Chemical & Engineering Data*, *35*(3), 253–257. <https://doi.org/10.1021/jc00061a009>
- Eek, M. K., Whittar, M. J., Bishop, J. K. B., & Wong, C. S. (1999). Influence of nutrients on carbon isotope fractionation by natural populations of Prymnesiophyte algae in NE Pacific. *Deep-Sea Research Part II: Topical Studies in Oceanography*, *46*(11–12), 2863–2876. [https://doi.org/10.1016/S0967-0645\(99\)00086-7](https://doi.org/10.1016/S0967-0645(99)00086-7)
- Falkowski, P. G., & Raven, J. A. (2007). *Aquatic photosynthesis* (2nd ed.). Princeton University Press.
- Farquhar, G. D., O'Leary, M. H., & Berry, J. A. (1982). On the relationship between carbon isotope discrimination and the intercellular carbon dioxide concentration in leaves. *Functional Plant Biology*, *9*(2), 121. <https://doi.org/10.1071/PP9820121>
- Fielding, S. R. (2013). *Emiliana huxleyi* specific growth rate dependence on temperature. *Limnology & Oceanography*, *58*(2), 663–666. <https://doi.org/10.4319/lo.2013.58.2.0663>
- Findlay, C. S., & Giraudeau, J. (2000). Extant calcareous nannoplankton in the Australian Sector of the Southern Ocean (austral summers 1994 and 1995). *Marine Micropaleontology*, *40*(4), 417–439. [https://doi.org/10.1016/S0377-8398\(00\)00046-3](https://doi.org/10.1016/S0377-8398(00)00046-3)
- Francois, R., Altabet, M. a., Goericke, R., McCorkle, D. C., Brunet, C., & Poisson, A. (1993). Changes in the $\delta^{13}C$ of surface water particulate organic matter across the subtropical convergence in the SW Indian Ocean. *Global Biogeochemical Cycles*, *7*(3), 627–644. <https://doi.org/10.1029/93GB01277>
- Freeman, K. H., & Hayes, J. M. (1992). Fractionation of carbon isotopes by phytoplankton and estimates of ancient CO_2 levels. *Global Biogeochemical Cycles*, *6*(2), 185–198. <https://doi.org/10.1029/92gb00190>
- Frenz, M., Baumann, K.-H., Boeckel, B., Hoppner, R., & Henrich, R. (2005). Quantification of foraminifer and coccolith carbonate in South Atlantic surface sediments by means of carbonate grain-size distributions. *Journal of Sedimentary Research*, *75*(3), 464–475. <https://doi.org/10.2110/jsr.2005.036>
- Fry, B., & Wainwright, S. C. (1991). Diatom sources of ^{13}C -rich carbon in marine food webs. *Marine Ecology Progress Series*, *76*(2), 149–157. <https://doi.org/10.3354/meps076149>
- Garcia, H., Weathers, K. W., Paver, C. R., Smolyar, I., Boyer, T. P., Locarnini, R. A., et al. (2019). *World Ocean Atlas 2018 Volume 2: Salinity* NOAA National Centers for Environmental Information (Vol. 82, pp. 50). NOAA Atlas NESDIS.

- Garcia, H. E., Weathers, K. W., Paver, C. R., Smolyar, I., Boyer, T. P., Locarnini, R. A., et al. (2019). *World Ocean Atlas 2018. Volume 4: Dissolved Inorganic Nutrients (Phosphate, Nitrate and Nitrate+Nitrite, Silicate)* (Vol. 84). NOAA Atlas NESDIS.
- Geitzenauer, K. R., Roche, M. B., & McIntyre, A. (1976). Modern pacific coccolith assemblages: Derivation and application to late Pleistocene paleotemperature analysis. *Memoirs-Geological Society of America*, *145*(1), 423–448. <https://doi.org/10.1130/MEM145-p423>
- Gould, J., Kienast, M., & Dowd, M. (2017). Investigation of the UK37' vs. SST relationship for Atlantic Ocean suspended particulate alkenones: An alternative regression model and discussion of possible sampling bias. *Deep Sea Research Part I: Oceanographic Research Papers*, *123*(August 2016), 13–21. <https://doi.org/10.1016/j.dsr.2017.02.007>
- Gould, J., Kienast, M., Dowd, M., & Schefuß, E. (2019). An open-ocean assessment of alkenone δD as a paleo-salinity proxy. *Geochimica et Cosmochimica Acta*, *246*, 478–497. <https://doi.org/10.1016/j.gca.2018.12.004>
- Hagino, K., & Okada, H. (2006). Intra- and infra-specific morphological variation in selected coccolithophore species in the equatorial and sub-equatorial Pacific Ocean. *Marine Micropaleontology*, *58*(3), 184–206. <https://doi.org/10.1016/j.marmicro.2005.11.001>
- Hagino, K., Okada, H., & Matsuoka, H. (2000). Spatial dynamics of coccolithophore assemblages in the Equatorial Western-Central Pacific Ocean. *Marine Micropaleontology*, *39*(1–4), 53–72. [https://doi.org/10.1016/S0377-8398\(00\)00014-1](https://doi.org/10.1016/S0377-8398(00)00014-1)
- Haidar, A. T., & Thierstein, H. R. (2001). Coccolithophore dynamics off Bermuda (N. Atlantic). *Deep-Sea Research Part II: Topical Studies in Oceanography*, *48*(8–9), 1925–1956. [https://doi.org/10.1016/S0967-0645\(00\)00169-7](https://doi.org/10.1016/S0967-0645(00)00169-7)
- Harada, N., Shin, K. H., Murata, A., Uchida, M., & Nakatani, T. (2003). Characteristics of alkenones synthesized by a bloom of *Emiliania huxleyi* in the Bering Sea. *Geochimica et Cosmochimica Acta*, *67*(8), 1507–1519. [https://doi.org/10.1016/S0016-7037\(02\)01318-2](https://doi.org/10.1016/S0016-7037(02)01318-2)
- Henderiks, J., & Pagani, M. (2007). Refining ancient carbon dioxide estimates: Significance of coccolithophore cell size for alkenone-based pCO_2 records. *Paleoceanography*, *22*(3), PA3202. <https://doi.org/10.1029/2006PA001399>
- Henderiks, J., & Pagani, M. (2008). Coccolithophore cell size and the Paleogene decline in atmospheric CO_2 . *Earth and Planetary Science Letters*, *269*(3–4), 575–584. <https://doi.org/10.1016/j.epsl.2008.03.016>
- Hernández-Almeida, I., Krumhardt, K. M., Zhang, H., & Stoll, H. M. (2020). Estimation of physiological factors controlling carbon isotope fractionation in coccolithophores in photic zone and core-top samples. *Geochemistry, Geophysics, Geosystems*, *21*(11), 1–29. <https://doi.org/10.1029/2020GC009272>
- Herrmann, S., Weller, A. F., Henderiks, J., & Thierstein, H. R. (2012). Global coccolith size variability in Holocene deep-sea sediments. *Marine Micropaleontology*, *82*(83), 1–12. <https://doi.org/10.1016/j.marmicro.2011.09.006>
- Horigome, M. T., Ziveri, P., Grelaud, M., Baumann, K.-H., Marino, G., & Mortyn, P. G. (2014). Environmental controls on the *Emiliania huxleyi* calcite mass. *Biogeosciences*, *11*(8), 2295–2308. <https://doi.org/10.5194/bg-11-2295-2014>
- Iglesias-Rodríguez, M. D., Schofield, O. M., Batley, J., Medlin, L. K., & Hayes, P. K. (2006). Intraspecific genetic diversity in the marine coccolithophore *Emiliania huxleyi* (Prymnesiophyceae): The use of microsatellite analysis in marine phytoplankton population studies. *Journal of Phycology*, *42*(3), 526–536. <https://doi.org/10.1111/j.1529-8817.2006.00231.x>
- Jasper, J. P., & Hayes, J. M. (1990). A carbon isotope record of CO_2 levels during the late Quaternary. *Nature*, *347*(6292), 462–464. <https://doi.org/10.1038/347462a0>
- Jasper, J. P., Hayes, J. M., Mix, A. C., & Prahl, F. G. (1994). Photosynthetic fractionation of ^{13}C and concentrations of dissolved CO_2 in the central equatorial Pacific during the last 255,000 years. *Paleoceanography*, *9*(6), 781–798. <https://doi.org/10.1029/94pa02116>
- Kameo, K., & Bralower, T. (2000). Neogene Calcareous Nannofossil biostratigraphy of sites 998, 999, and 1000, Caribbean Sea. *Proceedings of the Ocean Drilling Program*, *165*, 3–17. <https://doi.org/10.2973/odp.proc.165.012.2000>
- Keeling, C. D. (1979). The Suess effect: ^{13}C Carbon- ^{14}C Carbon interrelations. *Environment International*, *2*(4–6), 229–300. [https://doi.org/10.1016/0160-4120\(79\)90005-9](https://doi.org/10.1016/0160-4120(79)90005-9)
- Key, R. M., Olsen, A., van Heuven, S., Lauvset, S. K., Velo, A., Lin, X., et al. (2015). *Global Ocean Data Analysis Project, Version 2 (GLODAPv2)*. *Global Ocean Data Analysis Project, Version 2 (GLODAPv2)*, ORNL/CDIAC-162, ND-P093. Carbon dioxide information analysis center: Oak Ridge National Laboratory, US Department of Energy. https://doi.org/10.3334/CDIAC/OTG.NDP093_GLODAPv2
- Kienast, M., MacIntyre, G., Dubois, N., Higginson, S., Normandeau, C., Chazen, C., & Herbert, T. D. (2012). Alkenone unsaturation in surface sediments from the eastern equatorial Pacific: Implications for SST reconstructions. *Paleoceanography*, *27*(1), PA1210. <https://doi.org/10.1029/2011PA002254>
- Kinkel, H., Baumann, K.-H., & Cepek, M. (2000). Coccolithophores in the equatorial Atlantic Ocean: Response to seasonal and Late Quaternary surface water variability. *Marine Micropaleontology*, *39*(1–4), 87–112. [https://doi.org/10.1016/S0377-8398\(00\)00016-5](https://doi.org/10.1016/S0377-8398(00)00016-5)
- Krumhardt, K. M., Lovenduski, N. S., Iglesias-Rodríguez, M. D., & Kleypas, J. A. (2017). Coccolithophore growth and calcification in a changing ocean. *Progress in Oceanography*, *159*(October), 276–295. <https://doi.org/10.1016/j.pocean.2017.10.007>
- Laws, E. A., Popp, B. N., Bidigare, R. R., Kennicutt, M. C., & Macko, S. A. (1995). Dependence of phytoplankton carbon isotopic composition on growth rate and $[CO_2]_{aq}$: Theoretical considerations and experimental results. *Geochimica et Cosmochimica Acta*, *59*(6), 1131–1138. [https://doi.org/10.1016/0016-7037\(95\)00030-4](https://doi.org/10.1016/0016-7037(95)00030-4)
- Laws, E. A., Popp, B. N., Bidigare, R. R., Riebesell, U., Burkhardt, S., & Wakeham, S. G. (2001). Controls on the molecular distribution and carbon isotopic composition of alkenones in certain haptophyte algae. *Geochemistry, Geophysics, Geosystems*, *2*(1), 1006. <https://doi.org/10.1029/2000GC000057>
- Laws, E. A., Popp, B. N., Cassar, N., & Tanimoto, J. (2002). ^{13}C discrimination patterns in oceanic phytoplankton: Likely influence of CO_2 concentrating mechanisms, and implications for palaeoreconstructions. *Functional Plant Biology*, *29*(3), 323. <https://doi.org/10.1071/PP01183>
- Locarnini, R. A., Mishonov, A. V., Baranova, O. K., Boyer, T. P., Zweng, M. M., Garcia, H. E., et al. (2019). *World Ocean Atlas 2018. Volume 1: Temperature* (Vol. 81). NOAA Atlas NESDIS.
- Lombard, F., da Rocha, R. E., Bijma, J., & Gattuso, J.-P. (2010). Effect of carbonate ion concentration and irradiance on calcification in planktonic foraminifera. *Biogeosciences*, *7*(1), 247–255. <https://doi.org/10.5194/bg-7-247-2010>
- Lueker, T. J., Dickson, A. G., & Keeling, C. D. (2000). Ocean pCO_2 calculated from dissolved inorganic carbon, alkalinity, and equations for K_1 and K_2 : Validation based on laboratory measurements of CO_2 in gas and seawater at equilibrium. *Marine Chemistry*, *70*(1–3), 105–119. [https://doi.org/10.1016/S0304-4203\(00\)00022-0](https://doi.org/10.1016/S0304-4203(00)00022-0)
- McClelland, H. L. O., Barbarin, N., Beaufort, L., Hermoso, M., Ferretti, P., Greaves, M., & Rickaby, R. E. M. (2016). Calcification response of a key phytoplankton family to millennial-scale environmental change. *Scientific Reports*, *6*, 1–11. <https://doi.org/10.1038/srep34263>
- McClelland, H. L. O., Bruggeman, J., Hermoso, M., & Rickaby, R. E. M. (2017). The origin of carbon isotope vital effects in coccolith calcite. *Nature Communications*, *8*(1), 14511. <https://doi.org/10.1038/ncomms14511>
- McGee, D., DeMenocal, P. B., Winckler, G., Stuut, J. B. W., & Bradtmiller, L. I. (2013). The magnitude, timing and abruptness of changes in North African dust deposition over the last 20,000 yr. *Earth and Planetary Science Letters*, *371*(372), 163–176. <https://doi.org/10.1016/j.epsl.2013.03.054>

- Müller, P. J., Kirst, G., Ruhland, G., von Storch, I., & Rosell-Melé, A. (1998). Calibration of the alkenone paleotemperature index $U_{37}^{K'}$ based on core-tops from the eastern South Atlantic and the global ocean (60°N–60°S). *Geochimica et Cosmochimica Acta*, 62(10), 1757–1772. [https://doi.org/10.1016/S0016-7037\(98\)00097-0](https://doi.org/10.1016/S0016-7037(98)00097-0)
- NASA Goddard Space Flight Center, Ocean Ecology Laboratory, & Ocean Biology Processing Group. (2018a). *Moderate-resolution Imaging Spectroradiometer (MODIS) aqua downwelling diffuse attenuation coefficient data; 2018 reprocessing*. <https://doi.org/10.5067/AQUA/MODIS/L3M/KD/2018>
- NASA Goddard Space Flight Center, Ocean Ecology Laboratory, & Ocean Biology Processing Group. (2018b). *Moderate-resolution Imaging Spectroradiometer (MODIS) aqua photosynthetically available radiation data; 2018 reprocessing*; NASA OB.DAAC. <https://doi.org/10.5067/AQUA/MODIS/L3M/PAR/2018>
- NASA Goddard Space Flight Center, Ocean Ecology Laboratory, & Ocean Biology Processing Group. (2018c). *Sea-viewing Wide Field-of-view Sensor (SeaWiFS) downwelling diffuse attenuation coefficient data; 2018 reprocessing*. <https://doi.org/10.5067/ORBVIEW-2/SEAWIFS/L3M/KD/2018>
- NASA Goddard Space Flight Center, Ocean Ecology Laboratory, & Ocean Biology Processing Group. (2018d). *Sea-viewing Wide Field-of-view Sensor (SeaWiFS) photosynthetically available radiation data; 2018 reprocessing*. Greenbelt. <https://doi.org/10.5067/ORBVIEW-2/SEAWIFS/L3M/PAR/2018>
- Ohkouchi, N., Kawamura, K., Kawahata, H., & Okada, H. (1999). Depth ranges of alkenone production in the central Pacific Ocean. *Global Biogeochemical Cycles*, 13(2), 695–704. <https://doi.org/10.1029/1998GB900024>
- Okada, H., & Honjo, S. (1973). The distribution of oceanic coccolithophores in the Pacific. *Deep-Sea Research*, 20(2748), 355–374. [https://doi.org/10.1016/0011-7471\(73\)90059-4](https://doi.org/10.1016/0011-7471(73)90059-4)
- Olsen, A., Key, R. M., Van Heuven, S., Lauvset, S. K., Velo, A., Lin, X., et al. (2016). The global ocean data analysis project version 2 (GLODAPv2)—An internally consistent data product for the world ocean. *Earth System Science Data*, 8(2), 297–323. <https://doi.org/10.5194/essd-8-297-2016>
- Olsen, A., Lange, N., Key, R. M., Tanhua, T., Álvarez, M., Becker, S., et al. (2019). GLODAPv2.2019—An update of GLODAPv2. *Earth System Science Data Discussions*, 11(April), 1–39. <https://doi.org/10.5194/essd-11-1437-2019>
- Pagani, M. (2014). Biomarker-based inferences of past climate: The alkenone pCO_2 proxy. In *Treatise on Geochemistry* (2nd ed., Vol. 12, pp. 361–378). Elsevier. <https://doi.org/10.1016/B978-0-08-095975-7.01027-5>
- Pagani, M., Arthur, M. A., & Freeman, K. H. (1999). Miocene evolution of atmospheric carbon dioxide. *Paleoceanography*, 14(3), 273–292. <https://doi.org/10.1029/1999PA900006>
- Pagani, M., Arthur, M. A., & Freeman, K. H. (2000). Variations in Miocene phytoplankton growth rates in the southwest Atlantic: Evidence for changes in ocean circulation. *Paleoceanography*, 15(5), 486–496. <https://doi.org/10.1029/1999PA000484>
- Pagani, M., Freeman, K. H., Ohkouchi, N., & Caldeira, K. (2002). Comparison of water column $[CO_2(aq)]$ with sedimentary alkenone-based estimates: A test of the alkenone- CO_2 proxy. *Paleoceanography*, 17(4), 21–1–21–12. <https://doi.org/10.1029/2002PA000756>
- Phelps, S. R., Hennon, G. M. M., Dyhrman, S. T., Hernández Limón, M. D., Williamson, O. M., & Polissar, P. J. (2021). Carbon isotope fractionation in Noelaerhabdaceae algae in culture and a critical evaluation of the alkenone paleobarometer. *Geochemistry, Geophysics, Geosystems*, 22(7), 1–20. <https://doi.org/10.1029/2021GC009657>
- Polissar, P. J., & D'Andrea, W. J. (2014). Uncertainty in paleohydrologic reconstructions from molecular δD values. *Geochimica et Cosmochimica Acta*, 129, 146–156. <https://doi.org/10.1016/j.gca.2013.12.021>
- Popp, B. N., Kenig, F., Wakeham, S. G., Laws, E. A., & Bidigare, R. R. (1998). Does growth rate affect ketone unsaturation and intracellular carbon isotopic variability in *Emiliania huxleyi*? *Paleoceanography*, 13(1), 35–41. <https://doi.org/10.1029/97PA02594>
- Popp, B. N., Laws, E. A., Bidigare, R. R., Dore, J. E., Hanson, K. L., & Wakeham, S. G. (1998). Effect of phytoplankton cell geometry on carbon isotopic fractionation. *Geochimica et Cosmochimica Acta*, 62(1), 69–77. [https://doi.org/10.1016/S0016-7037\(97\)00333-5](https://doi.org/10.1016/S0016-7037(97)00333-5)
- Popp, B. N., Takigiku, R., Hayes, J. M., Louda, J., & Baker, E. W. (1989). The post-paleozoic chronology and mechanism of ^{13}C depletion in primary marine organic matter. *American Journal of Science*, 289, 436–454. <https://doi.org/10.2475/ajs.289.4.436>
- Poulton, A. J., Holligan, P. M., Charalampopoulou, A., & Adey, T. R. (2017). Coccolithophore ecology in the tropical and subtropical Atlantic Ocean: New perspectives from the Atlantic meridional transect (AMT) programme. *Progress in Oceanography*, 158, 150–170. <https://doi.org/10.1016/j.pocean.2017.01.003>
- Prahl, F. G., Mix, A. C., & Sparrow, M. A. (2006). Alkenone paleothermometry: Biological lessons from marine sediment records off western South America. *Geochimica et Cosmochimica Acta*, 70(1), 101–117. <https://doi.org/10.1016/j.gca.2005.08.023>
- Prahl, F. G., Popp, B. N., Karl, D. M., & Sparrow, M. A. (2005). Ecology and biogeochemistry of alkenone production at Station ALOHA. *Deep-Sea Research Part I: Oceanographic Research Papers*, 52(5), 699–719. <https://doi.org/10.1016/j.dsr.2004.12.001>
- Raja, M., & Rosell-Melé, A. (2021). Appraisal of sedimentary alkenones for the quantitative reconstruction of phytoplankton biomass. *Proceedings of the National Academy of Sciences of the United States of America*, 118(2), 1–7. <https://doi.org/10.1073/pnas.2014787118>
- Rau, G. H., Riebesell, U., & Wolf-Gladrow, D. (1996). A model of photosynthetic ^{13}C fractionation by marine phytoplankton based on diffusive molecular CO_2 uptake. *Marine Ecology Progress Series*, 133, 275–285. <https://doi.org/10.3354/meps133275>
- Rau, G. H., Takahashi, T., & Des Marais, D. J. (1989). Latitudinal variations in plankton $\delta^{13}C$: Implications for CO_2 and productivity in past oceans. *Nature*, 341(6242), 516–518. <https://doi.org/10.1038/341516a0>
- Rau, G. H., Takahashi, T., Desmarais, D. J., Repeta, D. J., & Martin, J. H. (1992). The relationship between delta ^{13}C of organic-matter and $[CO_2(aq)]$ in Ocean surface-water: Data from a JGOFS site in the northeast Atlantic-Ocean and a model. *Geochimica et Cosmochimica Acta*, 56, 1413–1419. [https://doi.org/10.1016/0016-7037\(92\)90073-R](https://doi.org/10.1016/0016-7037(92)90073-R)
- Riebesell, U., Burkhardt, S., Dauelsberg, A., & Kroon, B. (2000). Carbon isotope fractionation by a marine diatom: Dependence on the growth-rate-limiting resource. *Marine Ecology Progress Series*, 193, 295–303. <https://doi.org/10.3354/meps193295>
- Riebesell, U., Revill, A. T., Holdsworth, D. G., & Volkman, J. K. (2000). The effects of varying CO_2 concentration on lipid composition and carbon isotope fractionation in *Emiliania huxleyi*. *Geochimica et Cosmochimica Acta*, 64(24), 4179–4192. [https://doi.org/10.1016/S0016-7037\(00\)00474-9](https://doi.org/10.1016/S0016-7037(00)00474-9)
- Rosell-Melé, A., & Prahl, F. G. (2013). Seasonality of $U_{37}^{K'}$ temperature estimates as inferred from sediment trap data. *Quaternary Science Reviews*, 72, 128–136. <https://doi.org/10.1016/j.quascirev.2013.04.017>
- Rost, B., Zondervan, I., & Riebesell, U. (2002). Light-dependent carbon isotope fractionation in the coccolithophorid *Emiliania huxleyi*. *Limnology & Oceanography*, 47(1), 120–128. <https://doi.org/10.4319/lo.2002.47.1.0120>
- Saavedra-Pellitero, M., & Baumann, K.-H. (2015). Comparison of living and surface sediment coccolithophore assemblages in the Pacific sector of the Southern Ocean. *Micropaleontology*, 61(6), 507–520.
- Saavedra-Pellitero, M., Baumann, K.-H., Flores, J.-A., & Gersonde, R. (2014). Biogeographic distribution of living coccolithophores in the Pacific sector of the Southern Ocean. *Marine Micropaleontology*, 109, 1–20. <https://doi.org/10.1016/j.marmicro.2014.03.003>

- Saavedra-Pellitero, M., Flores, J.-A., Baumann, K.-H., & Sierro, F. J. (2010). Coccolith distribution patterns in surface sediments of Equatorial and Southeastern Pacific Ocean. *Geobios*, 43(1), 131–149. <https://doi.org/10.1016/j.geobios.2009.09.004>
- Schiebel, R., Brupbacher, U., Schmidtko, S., Nausch, G., Waniek, J. J., & Thierstein, H. R. (2011). Spring coccolithophore production and dispersion in the temperate eastern North Atlantic Ocean. *Journal of Geophysical Research: Oceans*, 116(8), C08030. <https://doi.org/10.1029/2010JC006841>
- Schiebel, R., Zeltner, A., Treppke, U. F., Waniek, J. J., Bollmann, J., Rixen, T., & Hemleben, C. (2004). Distribution of diatoms, coccolithophores and planktic foraminifers along a trophic gradient during SW monsoon in the Arabian Sea. *Marine Micropaleontology*, 51(3–4), 345–371. <https://doi.org/10.1016/j.marmicro.2004.02.001>
- Schmittner, A., Gruber, N., Mix, A. C., Key, R. M., Tagliabue, A., & Westberry, T. K. (2013). Biology and air-sea gas exchange controls on the distribution of carbon isotope ratios ($\delta^{13}\text{C}$) in the ocean. *Biogeosciences*, 10(9), 5793–5816. <https://doi.org/10.5194/bg-10-5793-2013>
- Schneider, N., & Müller, P. (1990). The meridional and seasonal structures of the mixed-layer depth and its diurnal amplitude observed during the Hawaii-to-Tahiti shuttle experiment. *Journal of Physical Oceanography*, 20(9), 1395–1404. [https://doi.org/10.1175/1520-0485\(1990\)020<1395:TMASSO>2.0.CO;2](https://doi.org/10.1175/1520-0485(1990)020<1395:TMASSO>2.0.CO;2)
- Schulte, S., Benthien, A., Andersen, N., Müller, P. J., Rühlemann, C., & Schneider, R. R. (2003). Stable carbon isotopic composition of the $\text{C}_{37:2}$ alkenone: A proxy for $\text{CO}_2(\text{aq})$ concentration in oceanic surface waters? In *The South Atlantic in the Late Quaternary* (Vol. 2, pp. 195–211): Springer Berlin Heidelberg. https://doi.org/10.1007/978-3-642-18917-3_10
- Schwab, C., Kinkel, H., Weinelt, M., & Repschläger, J. (2012). Coccolithophore paleoproductivity and ecology response to deglacial and Holocene changes in the Azores Current System. *Paleoceanography*, 27(3), PA3210. <https://doi.org/10.1029/2012PA002281>
- Sikes, E. L., Farrington, J. W., & Keigwin, L. D. (1991). Use of the alkenone unsaturation ratio U_{37}^k to determine past sea surface temperatures: Core-top SST calibrations and methodology considerations. *Earth and Planetary Science Letters*, 104, 36–47. [https://doi.org/10.1016/0012-821X\(91\)90235-A](https://doi.org/10.1016/0012-821X(91)90235-A)
- Sikes, E. L., Volkman, J. K., Robertson, L. G., & Pichon, J.-J. (1997). Alkenones and alkenes in surface waters and sediments of the Southern Ocean: Implications for paleotemperature estimation in polar regions. *Geochimica et Cosmochimica Acta*, 61(7), 1495–1505. [https://doi.org/10.1016/S0016-7037\(97\)00017-3](https://doi.org/10.1016/S0016-7037(97)00017-3)
- Sonzogni, C., Bard, E., Rostek, F., Lafont, R., Rosell-Mele, A., & Eglinton, G. (1997). Core-top calibration of the alkenone index vs sea surface temperature in the Indian Ocean. *Deep-Sea Research Part II: Topical Studies in Oceanography*, 44(6–7), 1445–1460. [https://doi.org/10.1016/S0967-0645\(97\)00010-6](https://doi.org/10.1016/S0967-0645(97)00010-6)
- Spero, H. J., & Lea, D. W. (1993). Intraspecific stable isotope variability in the planktic foraminifera *Globigerinoides sacculifer*: Results from laboratory experiments. *Marine Micropaleontology*, 22(3), 221–234. [https://doi.org/10.1016/0377-8398\(93\)90045-Y](https://doi.org/10.1016/0377-8398(93)90045-Y)
- Stoll, H. M., Guitian, J., Hernandez-Almeida, I., Mejia, L. M., Phelps, S. R., Polissar, P. J., et al. (2019). Upregulation of phytoplankton carbon concentrating mechanisms during low CO_2 glacial periods and implications for the phytoplankton pCO_2 proxy. *Quaternary Science Reviews*, 208, 1–20. <https://doi.org/10.1016/j.quascirev.2019.01.012>
- Takahashi, T., Sutherland, S. C., Chipman, D. W., Goddard, J. G., Ho, C., Newberger, T., et al. (2014). Climatological distributions of pH, pCO_2 , total CO_2 , alkalinity, and CaCO_3 saturation in the global surface ocean, and temporal changes at selected locations. *Marine Chemistry*, 164, 95–125. <https://doi.org/10.1016/j.marchem.2014.06.004>
- Takayama, T. (1993). Notes on Neogene calcareous nanofossil biostratigraphy of the Ontong Java plateau and size variations of Reticulofenestra coccoliths. *Proceedings of the Ocean Drilling Program, Scientific Results*, 130(11), 179–229.
- Tanner, T., Hernández-Almeida, I., Drury, A. J., Guitián, J., & Stoll, H. (2020). Decreasing atmospheric CO_2 during the late miocene cooling. *Paleoceanography and Paleoclimatology*, 35(12), e2020PA003925. <https://doi.org/10.1029/2020PA003925>
- Tierney, J. E., & Tingley, M. P. (2018). BAYSPLINE: A New calibration for the alkenone paleothermometer. *Paleoceanography and Paleoclimatology*, 33(3), 281–301. <https://doi.org/10.1002/2017PA003201>
- Tolosa, I., Miquel, J.-C., Gasser, B., Raimbault, P., Azouzi, L., & Claustre, H. (2008). Ecology and biogeochemistry of contrasting trophic environments in the South East Pacific by carbon isotope ratios on lipid biomarkers. *Biogeosciences Discussions*, 4(6), 4653–4696. <https://doi.org/10.5194/bgd-4-4653-2007>
- Uppström, L. R. (1974). The boron/chlorinity ratio of deep-sea water from the Pacific Ocean. *Deep-Sea Research and Oceanographic Abstracts*, 21(2), 161–162. [https://doi.org/10.1016/0011-7471\(74\)90074-6](https://doi.org/10.1016/0011-7471(74)90074-6)
- Van Heuven, S., Pierrot, D., Rae, J. W. B., Lewis, E., & Wallace, D. W. R. (2011). MATLAB program developed for CO_2 system calculations. In *Carbon dioxide information analysis center: Oak Ridge National Laboratory, U.S. Department of Energy*. https://doi.org/10.3334/CDIAC/otg.CO2SYS_MATLAB_v1.1
- Verity, P. G., Robertson, C. Y., Tronzo, C. R., Andrews, M. G., Nelson, J. R., & Sieracki, M. E. (1992). Relationships between cell volume and the carbon and nitrogen content of marine photosynthetic nanoplankton. *Limnology & Oceanography*, 37(7), 1434–1446. <https://doi.org/10.4319/lo.1992.37.7.1434>
- Villiot, N., Poulton, A. J., Butcher, E. T., Daniels, L. R., & Coggins, A. (2021). Allometry of carbon and nitrogen content and growth rate in a diverse range of coccolithophores. *Journal of Plankton Research*, 00(00), 1–526. <https://doi.org/10.1093/plankt/fbab038>
- Wallsgrave, R. J. (2008). *Alkenone-producing algae as a function of specific growth*. University of Hawaii at Manoa.
- Weiss, R. F. (1974). Carbon dioxide in water and seawater: The solubility of a non-ideal gas. *Marine Chemistry*, 2(3), 203–215. [https://doi.org/10.1016/0304-4203\(74\)90015-2](https://doi.org/10.1016/0304-4203(74)90015-2)
- Wilkes, E. B., Lee, R. B. Y., McClelland, H. L. O., Rickaby, R. E. M., & Pearson, A. (2018). Carbon isotope ratios of coccolith-associated polysaccharides of *Emiliania huxleyi* as a function of growth rate and CO_2 concentration. *Organic Geochemistry*, 119, 1–10. <https://doi.org/10.1016/j.orggeochem.2018.02.006>
- Wilkes, E. B., & Pearson, A. (2019). A general model for carbon isotopes in red-lineage phytoplankton: Interplay between unidirectional processes and fractionation by RubisCO. *Geochimica et Cosmochimica Acta*, 265, 163–181. <https://doi.org/10.1016/j.gca.2019.08.043>
- Wolfshorndl, M., Danford, R., & Sachs, J. P. (2019). 2H/1H fractionation in microalgal lipids from the North Pacific Ocean: Growth rate and irradiance effects. *Geochimica et Cosmochimica Acta*, 246, 317–338. <https://doi.org/10.1016/j.gca.2018.11.027>
- Wolhowe, M. D., Prahl, F. G., Langer, G., Oviedo, A. M., & Ziveri, P. (2015). Alkenone δD as an ecological indicator: A culture and field study of physiologically-controlled chemical and hydrogen-isotopic variation in C_{37} alkenones. *Geochimica et Cosmochimica Acta*, 162, 166–182. <https://doi.org/10.1016/j.gca.2015.04.034>
- Wolhowe, M. D., Prahl, F. G., White, A. E., Popp, B. N., & Rosas-Navarro, A. (2014). A biomarker perspective on coccolithophorid growth and export in a stratified sea. *Progress in Oceanography*, 122, 65–76. <https://doi.org/10.1016/j.pocean.2013.12.001>
- Yamamoto, M., Shimamoto, A., Fukuhara, T., Naraoka, H., Tanaka, Y., & Nishimura, A. (2007). Seasonal and depth variations in molecular and isotopic alkenone composition of sinking particles from the western North Pacific. *Deep Sea Research Part I: Oceanographic Research Papers*, 54(9), 1571–1592. <https://doi.org/10.1016/j.dsr.2007.05.012>

- Young, J. R. (1990). Size variation of Neogene Reticulofenestra coccoliths from Indian Ocean DSDP Cores. *Journal of Micropalaeontology*, 9(1), 71–85. <https://doi.org/10.1144/jm.9.1.71>
- Young, J. R., Bown, P. R., & Lees, J. A. (2017). *Nannotax3 website*. Retrieved from <http://www.mikrotax.org/Nannotax3/>
- Zhang, Y., Bach, L. T., Schulz, K. G., & Riebesell, U. (2015). The modulating effect of light intensity on the response of the coccolithophore *Gephyrocapsa oceanica* to ocean acidification. *Limnology & Oceanography*, 60(6), 2145–2157. <https://doi.org/10.1002/lno.10161>
- Zhang, Y. G., Henderiks, J., & Liu, X. (2020). Refining the alkenone-pCO₂ method II: Towards resolving the physiological parameter 'b'. *Geochimica et Cosmochimica Acta*, 281, 118–134. <https://doi.org/10.1016/j.gca.2020.05.002>
- Zhang, Y. G., Pearson, A., Benthien, A., Dong, L., Huybers, P., Liu, X., & Pagani, M. (2019). Refining the alkenone-pCO₂ method I: Lessons from the Quaternary glacial cycles. *Geochimica et Cosmochimica Acta*, 260, 177–191. <https://doi.org/10.1016/j.gca.2019.06.032>

References From the Supporting Information

- Aristegui, J., Barton, E. D., Álvarez-Salgado, X. A., Santos, A. M. P., Figueiras, F. G., Kifani, S., et al. (2009). Sub-regional ecosystem variability in the Canary Current upwelling. *Progress in Oceanography*, 83(1–4), 33–48. <https://doi.org/10.1016/j.pocean.2009.07.031>
- Balch, W. M., Holligan, P. M., & Kilpatrick, K. A. (1992). Calcification, photosynthesis and growth of the bloom-forming coccolithophore, *Emiliania huxleyi*. *Continental Shelf Research*, 12(12), 1353–1374. [https://doi.org/10.1016/0278-4343\(92\)90059-S](https://doi.org/10.1016/0278-4343(92)90059-S)
- Bendif, E. M., Probert, I., Carmichael, M., Romac, S., Hagino, K., & de Vargas, C. (2014). Genetic delineation between and within the widespread coccolithophore morpho-species *Emiliania huxleyi* and *Gephyrocapsa oceanica* (Haptophyta). *Journal of Phycology*, 50(1), 140–148. <https://doi.org/10.1111/jpy.12147>
- Bruland, K. W., Middag, R., & Lohan, M. C. (2014). Controls of trace metals in seawater. In *Treatise on Geochemistry* (2nd ed., Vol. 8, pp. 19–51). Elsevier. <https://doi.org/10.1016/B978-0-08-095975-7.00602-1>
- Calil, P. H. R., Doney, S. C., Yumimoto, K., Eguchi, K., & Takemura, T. (2011). Episodic upwelling and dust deposition as bloom triggers in low-nutrient, low-chlorophyll regions. *Journal of Geophysical Research*, 116(C6), C06030. <https://doi.org/10.1029/2010JC006704>
- Clegg, S. L., & Sarmiento, J. L. (1989). The hydrolytic scavenging of metal ions by marine particulate matter. *Progress in Oceanography*, 23(1), 1–21. [https://doi.org/10.1016/0079-6611\(89\)90023-2](https://doi.org/10.1016/0079-6611(89)90023-2)
- Codispoti, L. (2000). *Hydrographic data: Temperature, salinity, nutrients from Niskin bottles*. Retrieved from <http://usjgofs.whoi.edu/jg/serv/jgofs/arabian/ttn-053/bottle.html>
- Engel, A., Zondervan, I., Aerts, K., Beaufort, L., Benthien, A., Chou, L., et al. (2005). Testing the direct effect of CO₂ concentration on a bloom of the coccolithophorid *Emiliania huxleyi* in mesocosm experiments. *Limnology & Oceanography*, 50(2), 493–507. <https://doi.org/10.4319/lo.2005.50.2.0493>
- Eppley, R. W., Rogers, J. N., & McCarthy, J. J. (1969). Half-saturation constants for uptake of nitrate and ammonium by marine phytoplankton¹. *Limnology & Oceanography*, 14(6), 912–920. <https://doi.org/10.4319/lo.1969.14.6.0912>
- Feng, Y., Roleda, M. Y., Armstrong, E., Boyd, P. W., & Hurd, C. L. (2017). Environmental controls on the growth, photosynthetic and calcification rates of a Southern Hemisphere strain of the coccolithophore *Emiliania huxleyi*. *Limnology & Oceanography*, 62(2), 519–540. <https://doi.org/10.1002/lno.10442>
- Hayes, J. M. (1993). Factors controlling 13C contents of sedimentary organic compounds: Principles and evidence. *Marine Geology*, 113(1–2), 111–125. [https://doi.org/10.1016/0025-3227\(93\)90153-M](https://doi.org/10.1016/0025-3227(93)90153-M)
- Hebel, D. (2018). *Bottle data from Cruise 32MW078-1, exchange version*. doi <https://doi.org/10.7284/907046>
- Henderiks, J. (2008). Coccolithophore size rules-Reconstructing ancient cell geometry and cellular calcite quota from fossil coccoliths. *Micropalaeontology*, 67(1–2), 143–154. <https://doi.org/10.1016/j.marmico.2008.01.005>
- Krishna, S., & Schartau, M. (2017). A data-model synthesis to explain variability in calcification observed during a CO₂ perturbation mesocosm experiment. *Biogeosciences*, 14(7), 1857–1882. <https://doi.org/10.5194/bg-14-1857-2017>
- Macias, D., Landry, M. R., Gershunov, A., Miller, A. J., & Franks, P. J. S. (2012). Climatic control of upwelling variability along the Western North-American coast. *PLoS One*, 7(1), 20–23. <https://doi.org/10.1371/journal.pone.0030436>
- Marra, J. (2002). *Photosynthetically available radiation (PAR)*. Retrieved from <http://usjgofs.whoi.edu/jg/serv/jgofs/arabian/PAR.html>
- Mook, W. G., Bommerson, J. C., & Staverman, W. H. (1974). Carbon isotope fractionation between dissolved bicarbonate and gaseous carbon dioxide. *Earth and Planetary Science Letters*, 22(2), 169–176. [https://doi.org/10.1016/0012-821X\(74\)90078-8](https://doi.org/10.1016/0012-821X(74)90078-8)
- Nanninga, H. J., & Tyrrell, T. (1996). Importance of light for the formation of algal blooms by *Emiliania huxleyi*. *Marine Ecology Progress Series*, 136(1–3), 195–203. <https://doi.org/10.3354/meps136195>
- Perrin, L., Probert, I., Langer, G., & Aloisi, G. (2016). Growth of the coccolithophore *Emiliania huxleyi* in light- and nutrient-limited batch reactors: Relevance for the BIOSOPE deep ecological niche of coccolithophores. *Biogeosciences*, 13(21), 5983–6001. <https://doi.org/10.5194/bg-13-5983-2016>
- Popp, B. N., Bidigare, R. R., Deschenes, B., Laws, E. A., Prahl, F. G., Tanimoto, J. K., & Wallsgrove, R. J. (2006). A new method for estimating growth rates of alkenone-producing haptophytes. *Limnology and Oceanography: Methods*, 4(4), 114–129. <https://doi.org/10.4319/lom.2006.4.114>
- Quay, P., & Stutsman, J. (2003). Surface layer carbon budget for the subtropical N. Pacific: Constraints at station ALOHA. *Deep Sea Research Part I: Oceanographic Research Papers*, 50(9), 1045–1061. [https://doi.org/10.1016/S0967-0637\(03\)00116-X](https://doi.org/10.1016/S0967-0637(03)00116-X)
- Raven, J. A., & Johnston, A. M. (1991). Mechanisms of inorganic-carbon acquisition in marine phytoplankton and their implications for the use of other resources. *Limnology & Oceanography*, 36(8), 1701–1714. <https://doi.org/10.4319/lo.1991.36.8.1701>
- Rohatgi, A. (2020). *Webplotdigitizer: Version 4.4*. Retrieved from <https://automeris.io/WebPlotDigitizer>
- Rosenberg, M. Bottle data from cruise 09AR19980228, exchange version. Retrieved from <https://cchdo.ucsd.edu/cruise/09AR19980228>
- Rost, B., Zondervan, I., & Riebesell, U. (2002). Light-dependent carbon isotope fractionation in the coccolithophorid *Emiliania huxleyi*. *Limnology & Oceanography*, 47(1), 120–128. <https://doi.org/10.4319/lo.2002.47.1.0120>
- Santiago-Mandujano, F. Bottle data from Cruise 32MW074_1, exchange version. Retrieved from <https://doi.org/10.7284/907042>
- Talley, L., & Swift, J. Bottle data from Cruise 316N145_7, exchange version. Retrieved from https://cchdo.ucsd.edu/cruise/316N145_7
- Tupas, L. Bottle data from Cruise 3230064_1, exchange version. Retrieved from <https://doi.org/10.7284/901339>
- Young, J. R., Geisen, M., Cros, L., Kleijne, A., Sprengel, C., Probert, I., & Østergaard, J. (2003). A guide to extant coccolithophore taxonomy. *Journal of Nannoplankton Research*, 125. (Special Issue 1).